# The Aqua-Matrix Universe: A Unified Field Synthesis from the Water Molecule to the Boundary of the Cosmos

Garrick Ramsey Holmes, RIFOR Affiliated Researcher, ORCID 0009-0008-9319-1518 · Nov 19, 2026

## Abstract

Space-time is not an abstract manifold. It is a physical medium: a continuous three-dimensional lattice of water molecules held together by asymmetric hydrogen bonds, one strong and one weak per molecule. The lattice is present in every state water occupies, it thins with density, and it never breaks in geometric character. This paper brings the full framework together in one place, from the single molecule to the boundary of the cosmos.

The refractive index of the lattice under radial strain reproduces the Schwarzschild metric and every classical test of general relativity. Laboratory water has already shown gravitational coupling that is frequency dependent, structure dependent and sign reversible (Hu et al., 2013). The same lattice, when bent, makes electric charge at a strength comparable to sensor ceramics (Wen et al., 2025), and the strain gradient that charges ice is the same quantity general relativity calls curvature. The lattice takes the form of vortex, torus and sphere at every scale where it has been measured, from a centimeter drop to the ring at the center of the galaxy. It sits inside every vacuum chamber ever built, which makes water the one variable never controlled in the double slit.

The universe is bounded. Its boundary is a near-perfect black body. It absorbs, it reflects, and it casts the shadow that makes the night sky black. An absorbing shell around the measured stellar population settles at 2.7244 K from luminosity and geometry alone, against the measured 2.72548 K of the cosmic microwave background. The boundary is the surface of a gravastar whose Israel junction conditions lock one day of interior time to one thousand years of exterior time. Helium, the second most abundant element, is the working gas: one exterior torus that pins the temperature floor at its lambda transition, carries the breathing of a sphere that expands and retracts, and supplies an interior force law of buoyancy in which flat rotation curves need no dark matter. Sagittarius A* is a resonant gravastar nested within the larger one. Cold Genesis theory derived the 17 MeV boson nine years before it was first reported.

The paper closes with every falsifiable prediction from the earlier work, each with the result that would make it fail, and one list that keeps what others measured apart from what this author proposes.

Keywords: water-matrix lattice, space-time, asymmetric hydrogen bonding, Schwarzschild metric, flexoelectricity, double slit, vortex, torus, bounded universe, Olbers' paradox, gravastar, Israel junction conditions, helium, Cold Genesis, X17, Sagittarius A*

## 1. Introduction: Field Synthesis and the One Variable

### 1.1 The silence at the center

General relativity describes gravity as curvature of a four-dimensional manifold. Every prediction has been confirmed to extraordinary precision. Yet the theory contains a silence at its center. Einstein's field

equations relate the curvature tensor to the stress-energy tensor. They say what space-time does. They do not say what space-time is made of.

Cosmology inherits that silence. The temperature of the void is attributed to a primordial fire, the flat rotation curves of galaxies to invisible mass, the acceleration seen in Type Ia supernovae to an unseen energy field. Each is a parameter purchased to cover a gap between observation and model. This paper proposes a complete alternative in which no such purchase is necessary.

The proposal is that space-time is the product of three inseparable quantities: water, frequency and gravity. The water-matrix lattice, a continuous physical network of water molecules connected by asymmetric hydrogen bonds, is the medium. Frequency is how energy moves through this medium. Gravity is the coupling between frequency and lattice structure. Remove any one, and the others have no physical meaning.

### 1.2 Field synthesis

Modern physics operates within disciplinary compartments. Oncology funds oncology. Fluid dynamics funds fluid dynamics. Cosmology funds cosmology. String theory develops in theoretical physics departments. Particle physics operates in accelerator facilities. Quantum biology investigates water in living systems. Astrophysical observations of water masers and compact objects proceed independently. Each compartment produces extraordinary results. The problem is not quality. The problem is isolation.

Results that are individually significant within their compartments may be collectively transformative when connected. The institutional structures of modern research do not reward connection. The researcher who publishes within a single field advances. The researcher who attempts to bridge fields belongs to none of them.

Field synthesis is the systematic identification of connections between results produced independently within these compartments. The method does not generate new experimental data. It reveals what becomes visible when existing results from different fields are placed in conversation rather than isolation. The natural world does not organize itself according to institutional boundaries. The water molecule forming hydrogen bonds in a laboratory flask operates through the same physics as the water molecule in an interstellar molecular cloud, a biological cell, or the boundary of a gravastar.

The scientists whose work appears throughout this paper built the foundation through careers of instrument construction, experimental execution and rigorous publication. Without their work there is nothing to synthesize. Nobody lied and nobody was careless. What this paper proposes is that coherence appears when their results are oriented toward the same physical substance.

### 1.3 The one variable

An experiment is only as good as its controls. When you run a test, you identify every single thing that could influence the outcome, and you hold all of them fixed except one. That one thing you allow to move is your variable. If you let two things change at once, you cannot say which one caused what. Every drug that works, every alloy that holds and every bridge that stands comes down to that discipline. Control everything. Vary one thing. Watch.

One substance sits inside every quantum experiment ever performed on Earth, at every pressure, in every apparatus, on every continent, in every decade. It has never been controlled, never isolated, never

deliberately varied, and in the most important versions of the experiment, never even measured. It is not exotic. It comes out of your tap. It is water.

The same substance carries 95 percent of Earth's tidal dissipation, charges thunderclouds when its ice bends, holds the spine of DNA, leaves icy moons as tori around their planets, and is detected in every astrophysical environment examined with sufficient sensitivity. This paper follows that one substance from the molecule outward and asks what it means that the same geometry appears at every scale.

### 1.4 How this paper is built

The paper proceeds from the smallest scale to the largest. Sections 2 to 4 set out the molecule, the strong-weak bonding rule and the lattice it builds, and the postulates. Sections 5 to 8 show the lattice as the substance of general relativity: the metric, the laboratory evidence, the unification of forces through frequency, and the planetary record of tidal dissipation. Section 9 gives the electric signature of the strained lattice in ice. Section 10 carries the lattice into living matter. Section 11 identifies the strings of string theory as hydrogen bonds. Section 12 treats the double slit and the vacuum chamber.

Sections 13 to 16 follow the vortex, the torus and the sphere from laboratory droplets through storms, poles, icy moons and the Earth-Moon system to water across the cosmos. Sections 17 to 24 develop the bounded universe: the shadow that makes the night sky black, the gravastar boundary, the 1,000-year day, helium as the working gas, the 350 nm boundary, the galactic center, Cold Genesis and the 17 MeV boson, and the strain now visible in the standard account. Sections 25 and 26 list every falsifiable prediction and separate what was measured from what is proposed. Section 27 sets out a theological interpretation, kept apart from the physics.

Every number can be checked with a calculator. Appendix A gives the full arithmetic toolkit. Throughout, the paper keeps two boxes. One holds what instruments measured. The other holds what this author proposes. Agreement between a model and data is not proof. The predictions in Section 25 are where this framework can fail.

## 2. The Molecule

### 2.1 The electron pairs build the shape

Oxygen has eight electrons. Two sit in an inner shell, close to the nucleus. That leaves six in the outer shell, two short of the eight that make a shell stable. Two hydrogen atoms, each carrying one electron, share with the oxygen, and everyone counts to eight. The bonds form.

Now count what is left on the oxygen. Six outer electrons, minus the two it shares with the hydrogens, leaves four electrons doing no bonding at all. They pair up into two lone pairs. Around the oxygen there are now four regions of negative charge: two shared pairs reaching toward the hydrogens and two lone pairs. Like charges repel, so each region moves as far from the other three as it can.

Four things pushed apart around a central point in three dimensions form a tetrahedron, a three-sided pyramid with every angle close to 109.5 degrees. Nobody designs this. It is what four mutually repelling regions do. The water molecule is not the flat cartoon drawn in school. It is a rigid three-dimensional pyramid, the $sp^3$ hybridization geometry. The geometry comes from the electron pairs first, and everything downstream inherits it.

## 2.2 Four docking sites

Oxygen pulls shared electrons toward itself. The two hydrogen tips are left slightly positive and the lone-pair side slightly negative. The molecule is a small pyramid that is also a four-pole magnet: two positive patches and two negative patches, at fixed positions and fixed angles.

Each molecule can therefore donate two hydrogen bonds from its hydrogen tips and accept two on its lone pairs. Two givers, two receivers, perfectly balanced. Any molecule meeting the lattice finds four points of attachment. Ammonia has three hydrogens to give but only one lone pair to receive, so a structure built from it tips and wanders. Hydrogen fluoride has one tip and three lone pairs, so it chains in one-dimensional strings. Among small molecules, water alone carries the two-and-two balance that allows an endless, repeating three-dimensional structure.

This balance shows itself in a fact too familiar to feel strange. Ice floats. Nearly every substance contracts as it freezes, so nearly every solid sinks in its own liquid. Water expands, because its tetrahedral network stays standing and the open pyramid geometry wins over tight packing. The lattice survives its own freezing.

## 2.3 The bond in free flight

The geometry belongs to the molecule, not to its surroundings. Two water molecules bonded in free flight, in a molecular beam with no liquid, no surface and no lattice beyond themselves, form a near-linear hydrogen bond directed at an acceptor angle of 57 ± 10 degrees (Dyke, Mack and Muenter, 1977). That is essentially half the tetrahedral angle, 109.47 ÷ 2 = 54.7 degrees. The bond aims along the lone-pair direction of the $sp^3$ geometry. Free flight is the sparsest state water can occupy, and the geometry still holds.

The bound structure persists in ordinary air. Rotationally resolved spectra of bound water have been recorded in equilibrium water vapor at room temperature (Tretyakov et al., 2013) and in atmospheric air (Serov et al., 2014), at an abundance of about one in a thousand.

## 2.4 No off switch

How close do two water molecules have to be before they attract? Common sense says attraction is a proximity effect, like two magnets that ignore each other across a room. That is not how it works.

The water molecule carries a permanent dipole of 1.85 debye in the vapor and about 2.95 debye in the condensed phase. On top of that permanent imbalance, the electron clouds of any two molecules fluctuate from moment to moment and set up momentary attractions of their own. London dispersion acts between any two polarizable molecules at any separation. It has no density threshold and no cutoff. It is why argon, chemically inert, still condenses.

There is no distance at which the attraction between water molecules switches off. Anywhere two water molecules exist in the same region of space, at any separation and any density, they are pulling toward each other: faintly when far, strongly when near, never zero. The pull is not a condition the environment grants them. It is a property they carry, like mass. Density is a number that says how many molecules a region contains. It changes nothing about the molecule's attraction for its own kind.

It follows that water has no disconnected state. A thin, scattered handful of water molecules is not an absence of structure. It is the same structure at lower density. Spread the molecules a meter apart and the network has not been deleted. It has been stretched. Sparse and absent are degrees of the same condition, and the condition is bondedness.

## 3. The Strong-Weak Rule and the Lattice That Never Breaks

### 3.1 One strong, one weak

Each water molecule donates two hydrogen bonds, one from each hydrogen tip. Of the two, one is strong and one is weak. Always one strong, one weak. If something strengthens one bond, the other bond on the same molecule weakens to compensate. The two are anti-correlated: a seesaw built into every molecule.

The rule was derived from first principles a decade before it was measured (Kühne and Khaliullin, 2013, 2014). It was measured directly by ultrafast two-dimensional infrared spectroscopy in December 2024: the two hydrogen bonds formed by one water molecule are markedly anti-correlated, and the anti-correlations are modulated by thermal motion and randomize in under 500 femtoseconds (Gunkel et al., 2024). The measurement was made on water diluted in dimethylformamide, where the bonds between water molecules are few. The anti-correlation produces non-random chain and ring structuring in nominally disordered liquid water.

The rule does not belong to the liquid, the ice, or any phase. It belongs to the molecule's bonding apparatus, the geometry of its lone pairs and hydrogens, and is therefore carried into every state the molecule enters. A rule that lives in the molecule cannot be destroyed by changing the molecule's address.

### 3.2 Every bond moves charge

In 2024 correlated vibrational spectroscopy isolated the signal of the hydrogen-bond stretch between interacting molecules in ordinary room-temperature water. Each hydrogen bond transfers about one fiftieth of an electron's charge between the bonded molecules (Flór et al., 2024). Hydroxide ions donate about 8 percent more negative charge to the network and hydronium ions accept about 4 percent less, so pH is a measured dial on charge flow through the lattice. Heavy water carries about 9 percent more hydrogen bonds than ordinary water, a measured isotope dial. No two molecules share identical bond sets, and the bonds are cooperative: one bond forming polarizes its partner and makes the next bond easier. The lattice is not a bag of independent handshakes. It is one connected network of charge.

The hydrogen bond is not a purely electrostatic attraction. Compton X-ray scattering on ice found that it has substantial covalent character, with electrons shared across it (Isaacs et al., 1999).

### 3.3 The repair mechanism

Half the connections being weak sounds like a flaw, like a builder announcing that half the bolts in a bridge are rated to snap. Now imagine that bridge in an earthquake. A structure of perfectly rigid members absorbs nothing and snaps. Towers in earthquake country are built with deliberate flex and sacrificial joints that yield and shed stress so the frame sways instead of shattering.

That is water. The strong bonds carry the load. The weak bonds are the sacrificial joints, popping loose and reconnecting elsewhere so stress drains out of the structure without cracking it. The bonds break and re-form about a trillion times per second (Gunkel et al., 2024). Put a disturbance into the water and the network loses its memory of it in about 50 femtoseconds (Cowan et al., 2005). Full randomization of the network takes about 2 picoseconds (Fayer, 2012). The wrecking ball moves in slow motion compared to the maintenance crew. You cannot hit this structure faster than it repairs.

Compressing liquid water does not break the network either. X-ray Raman measurements show that the density increase on compression comes from interstitial water generated inside a persisting tetrahedral network (Förster et al., 2024). The network holds while density changes inside it.

### 3.4 Through both critical points

Water has two critical points, one hot and one cold.

The cold critical point. When water is supercooled and compressed, its two liquid forms, high density and low density, merge. In 2026 femtosecond X-ray laser probing of supercooled water observed the liquid-liquid transition vanish and a critical state emerge at 210 ± 8 K and about 1,000 bar (You et al., 2026). Structural analysis resolves liquid water into two dominant local arrangements (Li et al., 2026). Ordinary room-temperature water already sits beyond this critical point, flickering between two packings. Through that transition the molecule keeps the same tetrahedral coordination of its neighbors. Two liquids, one geometry.

The hot critical point. Past 647 K and 22.1 MPa, liquid and gas cease to be distinct. For decades the assumption was that in this fog the molecules ricochet at random. Measurement says otherwise. X-ray Raman scattering of supercritical water at 380 °C and 300 bar finds about 65 percent of the molecules still hydrogen bonded, holding four intact bonds in tetrahedral patches (Wernet et al., 2005). Inelastic X-ray scattering finds the fast collective sound of hydrogen-bonded water, about 3 kilometers per second, carried into the supercritical state (Sun et al., 2020). Bound water structure is present in the vapor spectra at 650 K and up to 110 atmospheres (Odintsova and Tretyakov, 2013). The network thins. It does not forget how to be a network.

### 3.5 Tension

Pull on water hard enough and its pressure goes negative. Water in microscopic quartz inclusions sustains pressures as low as −140 MPa before it breaks by cavitation (Azouzi et al., 2013), and an experimental equation of state now runs down to −120 MPa (Pallares et al., 2016). Water stretched like a rope under a load no rope should survive holds together. Stretching orders the lattice: hydrogen-bond lifetimes lengthen, the tetrahedral structure strengthens and diffusion slows, right up to the moment the liquid tears.

### 3.6 The molecule survives a star

Water vapor is measured line by line in the dark cores of sunspots. It was first reported in 1970 (Mallia, Blackwell and Petford, 1970). In 1995 the infrared spectrum of hot water from the laboratory was matched to sunspot spectra recorded with the Kitt Peak Fourier transform spectrometer, and most of the unassigned sunspot lines were identified as water (Wallace et al., 1995). The assignments were

completed against millions of calculated lines at about 3,200 K (Polyansky et al., 1997). Wherever the temperature dips below the point at which the atoms come apart, the bonding rule resumes building.

### 3.7 Coherence in every state, measured

The record below is laboratory measurement only, grouped by the state the water was in. In every entry the instruments recorded water acting as one connected structure. Where a paper reads its data as pairs or small clusters, that reading is the authors' own; the table lists what was measured.

| State | What was measured | Source |
|---|---|---|
| Liquid, between protein samples | A coherent signal between samples 40.0 mm apart, carried on the water bending mode at 1,622 $cm^{-1}$ and its fourth overtone at 6,488 $cm^{-1}$ | bioRxiv, 2026 |
| Liquid in 2 to 20 nm gaps | The terahertz refractive index departs strongly from bulk; the network dynamics reach farther than expected | Science Advances, 2024 |
| Electrolyte solutions | The field of the ions changes water-to-water orientation over tens of hydration shells | Dedic et al., 2019 |
| Bulk liquid | Collective orientational order over 5 to 15 nm, visible from micromolar salt, the same for more than 20 electrolytes, in $H_2O$ and in $D_2O$ | Chen et al., 2016 |
| Bulk liquid | Molecular orientation correlated out to about 2 micrometers, falling as $r^{-3}$ | Shelton, 2014, 2015 |
| Liquid at 294 K | A collective excitation at 3,200 to 3,300 m/s, the speed of sound in ice | Sette et al., 1995 |
| Liquid | A coherent O-H stretch wave packet with a 10 fs period and 25 fs damping; the damping marks the coupling through the network | Giovannetti et al., 2026 |
| Liquid | A hydrogen atom pulls the oxygen of its neighbor closer and then pushes it away, observed directly by electron diffraction | Yang et al., 2021 |
| Liquid | $D_2O$ reorients about 30 percent slower than $H_2O$, while $^{16}O$ to $^{18}O$ changes it about 5 percent | Melillo and Cerveny, 2026 |
| Liquid in an optical cavity | The whole ensemble reorganizes together, and the network holds off thermal disordering | ChemRxiv, 2026 |
| Liquid with trace water | Trace water strengthens network connectivity, rebuilds fragmented networks and carries protons through them | Liu et al., 2026 |

| State | What was measured | Source |
|---|---|---|
| Air-water interface | Nanoclusters about 50 nm across, bounded by ice-like walls about 10 nm thick, with dielectric constants near 3.6 and 7.6 | Interfacial water nanoclusters, 2026 |
| Living plant xylem | Exclusion-zone water inside and outside the vessels, with potentials down to −200 mV | Wang and Pollack, 2024 |
| Next to Nafion | A negatively charged zone and a positive proton zone, both responding to infrared light | Sains Malaysiana, 2025 |
| Around hydrophilic particles | A cell-like structured zone about 100 micrometers wide, with charge separation at the interface | PLOS ONE, 2018 |
| Amorphous solid water | Above 130 K the second coordination shell grows; above 140 K the solid orders into stacking-disordered ice I | J. Phys. Chem. B, 2021 |
| Single molecules in beryl channels | Molecules too far apart to hydrogen bond still couple by dipole forces and show a ferroelectric soft mode | Gorshunov et al., 2016 |
| Molecules in cordierite pores | Ferroelectric domains, with order setting in near 3 K | Belyanchikov et al., 2022 |
| One molecule per $C_{60}$ cage | Coherent rotation lasting beyond 10 ps below about 100 K at the frequencies of free water; molecules in neighboring cages take part in spin conversion | Zhukov et al., 2020; Goh et al., 2014; Beduz et al., 2012 |
| Trimer on salt at $10^{-11}$ Torr | Three protons tunnel together | Kim, Han and Shin, 2025 |
| Tetramer on NaCl | Four protons tunnel in a concerted way; replacing H with D drops the rate at least a hundredfold | Meng et al., 2015; Feng et al., 2018 |
| Free clusters in molecular beams | Networks build from two molecules up to ten, turn three-dimensional at six, and tunnel as a whole | Keutsch and Saykally, 2001 |
| Free hexamer | A cage of six molecules with eight hydrogen bonds; in the prism, tunneling breaks two bonds at once | Liu, Brown and Saykally, 1997; Richardson et al., 2016 |
| Free pentamer and octamer | Three-dimensional networks appear at five molecules; the eight-molecule cube is resolved in 99 transitions | Zhang et al., 2020; Li et al., 2020; Cole et al., 2016 |
| Pure vapor, 285 to 332 K | Self-continuum absorption rising with the square of the vapor pressure | Toureille et al., 2026 |

| State | What was measured | Source |
|---|---|---|
| Vapor at about 60 °C | The rotation of one molecule shifts the rotational frequency of another, with signals lasting about 100 ps | Zhang et al., 2021 |
| Vapor and liquid | Coherent single-molecule rotation in the vapor; in the liquid the field drives collective rotation and the energy moves through the network | Elgabarty et al., 2020 |
| Water in nanocapsules | Water held in cucurbituril capsules, tracked at room temperature and up to 120 °C | Hwang et al., 2022 |
| $D_2O$ ice Ih | Hidden one-dimensional strings of order in the hydrogen network; librational phonons split near 68 meV | Chen et al., 2025 |
| $H_2O$ ice near 20 K | A dielectric anomaly with about 2 K of hysteresis, absent in $D_2O$ ice | Yen and Gao, 2015 |
| Ice Ih and Ic down to 5 K | A localized hydrogen jump of 0.75 Å at $2.7 \times 10^{11}$ per second, absent in ordered ice VIII and hindered by 20 percent deuteration | Bove et al., 2009 |
| Ice up to 50 GPa | Thermal conductivity rises to 20 GPa and then falls, traced to collective proton tunneling loops spanning nanometers | Wang et al., 2024 |
| Ice up to 97 GPa | A proton tunneling mode present at every pressure, into ice X | Meier et al., 2018 |
| High-density amorphous ice | Collective dynamics followed through the coherent X-ray signal | Karina et al., 2025 |
| Low-density amorphous ice | The intermolecular peak that crystal ice owes to long-range dipole interaction, present in the glass | Fukazawa, Ikeda and Suzuki, 2001 |

The same result comes from independent laboratories with different instruments. Concerted proton tunneling in water networks has been seen by neutron scattering in ice, by scanning tunneling microscopy in surface clusters, by beam spectroscopy in free clusters, by thermal conductivity and by NMR in compressed ice, by dielectric spectroscopy of bulk ice, and by single-crystal neutron scattering of the hydrogen chains: eight methods, in every state from the free cluster to compressed ice. $H_2O$ against $D_2O$ is a measured dial in five of them.

### 3.8 The record in one line

Boiled past the point where liquid exists, geometry intact. Split into two liquids, geometry intact. Compressed, network persisting. Stretched to tearing, holding. Heated to sunspot temperatures, the molecule surviving. Rebuilding itself a trillion times a second. A material with two critical points and one enduring geometry is not an enigma. It is a lattice.

## 4. The Postulates

### 4.1 Three postulates

The invariant bonding rule at the molecular scale produces a continuous lattice extending from planetary oceans through atmospheric vapor to interstellar molecular clouds. The spacing between molecules changes with density. The bonding rule does not. The lattice exists at the density of the ocean, about $3.3 \times 10^{22}$ molecules per cubic centimeter, and in the diffuse interstellar medium at fewer than one molecule per cubic centimeter. Water has been detected in every astrophysical environment examined with sufficient sensitivity.

Postulate 1. Space-time is identical to a three-dimensional lattice of water molecules connected by asymmetric hydrogen bonds: the water-matrix.

Postulate 2. All gravitational, relativistic and quantum phenomena arise from the geometry, density gradients and frequency dynamics of this lattice. No separate geometric manifold is required.

Postulate 3. The lattice is not a passive medium in which gravity acts. The lattice is gravity. The structural deformation of water under mass-energy strain, mediated by frequency, is what we measure and call gravity.

### 4.2 The relationship

Frequency + $H_2O$ + Gravity = Space-Time

These three quantities are not independent. They are co-constitutive. The medium determines which frequencies propagate and how they couple. The frequencies determine the gravitational behavior of the medium. The gravitational coupling determines the geometry of the medium. This circular, self-consistent determination is space-time.

It follows that there is no true vacuum. A region called empty is a region where the lattice is sparse. Section 12 shows that no water-free volume has ever been produced on Earth, by any method, at any pressure.

### 4.3 Objections answered

Lorentz invariance. A physical lattice might seem to define a preferred reference frame. That objection applies to rigid lattices. The water-matrix is not rigid. The bonding rule is defined locally at each node: each molecule forms one strong and one weak bond with its immediate neighbors whatever frame the observation is made in. The lattice has no global rest frame because it has no global rigid structure. It flows, stretches, compresses and reorganizes continuously. The luminiferous aether was abandoned because no experiment detected motion through a rigid frame. The failure to detect a rigid mechanical aether does not prove the absence of a medium. It proves the medium is not a rigid mechanical frame.

Extreme sparseness. In the most diffuse intergalactic regions water may fall below one molecule per cubic meter. The relevant quantity is not number density but the persistence of the bonding rule. Every water molecule that exists follows the same rule. The lattice thins; the geometry at each node remains. Where the lattice thins toward absence, gravitational coupling should thin with it. That is not a weakness of the framework. It is a prediction (Section 25).

Extreme heat. Above about 2,500 K, in accretion disks, stellar interiors and the hot gas of galaxy clusters, water molecules dissociate. The constituent hydrogen and oxygen remain. If the lattice is fundamental and particles are excitations within it, dissociation is a phase transition of the lattice, not its destruction. The lattice enters a plasma phase in which the bonding geometry changes while its elements persist, and the bonding rule resumes wherever the temperature falls (Section 3.6). The framework predicts that gravitational coupling in such environments differs systematically from environments where the molecular lattice is intact.

Composition. The objection that water cannot be fundamental because it is made of hydrogen and oxygen, themselves made of smaller particles, inverts the proposed order. In this framework the lattice is fundamental and particles are vibrational modes within it. Water molecules are the nodes of the lattice. Their substructure is the internal degrees of freedom of those nodes. The hierarchy runs from lattice to node to substructure.

General relativity. The water-matrix does not replace general relativity. It identifies the physical substrate general relativity describes. Einstein's field equations remain valid as the mathematical description of how the lattice responds to mass-energy. The Schwarzschild and Kerr metrics remain valid as solutions. What changes is the interpretation: the manifold is not abstract geometry but a physical medium, the curvature tensor describes the strain of that medium, and the geodesic equation describes the path of least optical length through the strained lattice. All of Einstein's tested predictions stand.

## 5. The Metric

### 5.1 The refractive index of the strained lattice

Consider a static, spherically symmetric concentration of mass M embedded in the water-matrix. The mass compresses the surrounding lattice, increasing local density and producing a radial strain field $\varepsilon(r)$ that falls with distance. That strain changes the speed at which signals propagate through the lattice, exactly as strain in any physical medium changes its refractive properties. Write the refractive index as $n(r) = 1 + \varepsilon(r)$.

For a signal propagating through a medium of index n, the time it experiences relative to a distant observer is dt divided by n. Identify this with the gravitational time dilation of the Schwarzschild solution:

$$d\tau/dt = 1/n(r) = \sqrt{(1 - 2GM/(c^2 r))}$$

This fixes the refractive index of the strained lattice:

$$n(r) = (1 - 2GM/(c^2 r))^{(-1/2)}$$

### 5.2 The line element

The line element for signal propagation through an isotropic medium with a spatially varying refractive index is

$$ds^2 = -(c^2/n^2(r))\, dt^2 + n^2(r)\, dr^2 + r^2\, d\Omega^2$$

Substituting n(r):

$ds^2 = -(1 - 2GM/(c^2 r))\, c^2\, dt^2 + (1 - 2GM/(c^2 r))^{(-1)}\, dr^2 + r^2\, d\Omega^2$

This is the Schwarzschild metric. It emerges from the refractive index of the water-matrix under radial strain, without the Ricci tensor or any abstract geometric construction. The metric describes the optical properties of a physical medium.

The strain has two readouts. The push: strain slows every process the lattice carries, which is the time part of the index. The stretch: the same strain stretches the lattice radially, which is the space part. A clock reads the push alone. Light reads the push and the stretch together.

### 5.3 The classical tests

Gravitational time dilation. Clocks in denser lattice run slower because every physical process propagates through a medium of higher index. The dilation factor follows from the lattice density profile. Confirmed by Pound and Rebka (1960), by Hafele and Keating (1972), and by the corrections applied continuously to GPS satellites.

Gravitational redshift. A photon leaving a mass passes from denser to sparser lattice. The index drops and the wavelength stretches in proportion. The frequency ratio between emission at $r_1$ and observation at $r_2$ is $n(r_2)/n(r_1)$. Confirmed by Pound and Rebka (1960) and by solar spectral measurements.

Light deflection. Light follows Fermat's principle through the graded-index lattice. The push alone gives a deflection of $2GM/c^2 b$, where b is the impact parameter. The stretch adds an equal amount, giving the full measured $4GM/c^2 b$. The factor of four arises because both the temporal and the spatial parts of the index enter the path. Confirmed by Dyson, Eddington and Davidson (1920) and by radio interferometry to high precision.

Perihelion precession. Orbits in the Schwarzschild metric carry a $1/r^3$ correction absent from Newtonian gravity. In the lattice this arises from velocity-dependent coupling with the density gradient: a body moving faster through denser lattice at perihelion couples more strongly than at aphelion. The precession per orbit is $6\pi GM/c^2 a(1 - e^2)$. For Mercury this is 43 arcseconds per century, the excess Le Verrier (1859) found and Clemence (1947) refined.

Shapiro delay. A radar signal passing near a mass travels through denser lattice and physically slows. The round-trip excess is $(4GM/c^3) \ln(4r_1 r_2/b^2)$. Proposed by Shapiro (1964) and confirmed by the Cassini spacecraft to about two parts in a hundred thousand (Bertotti, Iess and Tortora, 2003).

Gravitational waves. Accelerating masses send compression and rarefaction through the lattice at a speed set by its bulk modulus and density. LIGO's detection confirmed propagation at c (Abbott et al., 2016).

All classical tests are recovered because the lattice produces the identical metric. The predictions are identical. The substrate is identified.

### 5.4 Rotation: the Kerr metric

A rotating mass drags the surrounding lattice into co-rotation, creating a vortex. The Fresnel drag coefficient, known since the nineteenth century, adds a cross term to the line element. Setting the lattice drag term equal to the frame-dragging term of the Kerr metric fixes the lattice angular velocity at

every point. In the weak field the lattice angular velocity falls off as $\Omega \propto 1/r^3$, the Lense-Thirring rate measured by Gravity Probe B (Everitt et al., 2011).

The ergosphere acquires a concrete physical meaning. It is the region where the lattice flow velocity exceeds the speed at which anything can propagate against the current. Objects are swept into co-rotation because they cannot move upstream faster than light. This is a fluid-mechanical criterion, not an abstract coordinate condition. The Earth's own rotation drags the lattice the same way, and the frame dragging Gravity Probe B measured is the lattice turning with the planet.

## 6. Gravity in Laboratory Water

This section presents the strongest category of evidence first, because it is experimental rather than theoretical, measured rather than derived, and published by independent groups with no connection to this framework. It precedes theory in this account because it precedes theory in authority.

### 6.1 Negative effective gravity

Hu, Yang, Zi, Chan and Ho (2013) built a water channel 8 millimeters deep, pierced by a periodic array of vertical split tubes acting as Helmholtz resonators. Each tube had an outer radius of 4 mm, an inner radius of 3 mm and a slit 1 mm wide, with the tubes spaced 12 mm apart. Waves outside each tube drove the water in the slit in and out, setting the water surface inside the tube vibrating at the resonant frequency.

For wave frequencies from 4.1 to 4.85 Hz, the effective gravitational acceleration experienced by water waves crossing the array became negative. A transmission dip appeared at 4.4 Hz where the effective gravity crossed below zero, and wave propagation was prohibited across the band. The effective gravity takes the form

$$g_e = g_o / (1 + f_s\, k_o^2 / (k_r^2 - k_o(k_o + i\, c_k)))$$

where $g_o$ is Earth's gravitational acceleration, $f_s$ the filling ratio of the resonators, $k_o$ the wavenumber, $k_r$ the resonant wavenumber and $c_k$ the radiation loss.

The experiment carried a control. The split tubes were replaced by rigid cylinders of the same outer radius. The rigid cylinders changed the effective depth and gravity in a simple way, $g_e = g_o/(1 - f_s)$, always positive. The dip disappeared and the waves passed freely. The negative gravity came from the resonant structure of the array, not from periodicity, not from scattering off obstacles, and not from any change to the water. The water was the same water. What changed was the frequency relationship between the wave and the structure it passed through.

This is the central experimental result for the framework. Gravitational coupling in water is not a fixed constant set by mass and distance alone. It is a function of frequency. Change which frequencies the structure supports and the coupling changes magnitude and sign. The medium determines which frequencies propagate. The frequencies determine the gravity. The gravity determines the geometry. This is the cycle that constitutes space-time. The result is about effective gravity for water waves, measured in water.

## 6.2 Horizons and superradiance in water

Unruh (1981) showed that the equation governing small disturbances in a moving fluid is mathematically identical to the Klein-Gordon equation for a field on a curved Lorentzian metric. The flow profile defines the metric. Regions where the flow outruns the wave speed are horizons.

Weinfurtner, Tedford, Penrice, Unruh and Lawrence (2011) built this in water. A flow over a weir passed from slower than the wave speed to faster, forming a white-hole horizon that surface waves cannot cross upstream. The spectrum of waves scattered from the horizon was thermal, with a temperature matching the surface gravity of the flow: stimulated Hawking emission, measured in water. The authors argue that this bears on spontaneous Hawking emission.

Torres, Patrick, Coutant, Richartz, Tedford and Weinfurtner (2017) built a draining vortex in a water tank. Waves meeting the vortex at certain angular momenta came out with more energy than they carried in, drawing energy from the rotating flow. This is rotational superradiance, the Penrose process around a spinning compact object, measured in a laboratory tank.

The standard reading treats these results as coincidence: water happens to obey the same equation, so it can serve as an analog computer. This framework's reading is simpler. Water produces gravitational physics because water is the medium in which gravitational physics operates. The analog gravity program has been running the diagnosis for two decades. The mathematics is not coincidental. It is diagnostic. Water does not imitate a horizon. A horizon in water is gravitational physics.

## 6.3 Water entering water

Zekri, Korobkin and Cooker (2021) analyzed the early stage of a symmetric body entering calm water and asked what gravity adds. Their conclusion is that gravity changes the water from a region of passive inertia into an active responder. The gravitational correction to the force on the body grows as $t^{3/2}$, so the longer the body interacts with the water the more the gravitational coupling dominates. The correction has a hydrostatic part, the weight of the water column, and a dynamic part, the change gravity makes to the flow itself, which adds about 6 percent beyond the hydrostatic prediction. Gravity raises the total force and at the same time shrinks the wetted contact region. Water under gravitational strain concentrates its coupling rather than spreading it.

## 6.4 Break the contact, lose the coupling

Whether a body stays connected to the water decides how the water acts on it. Two spheres identical except for a nanometric surface coating, one wetting and one water-repellent, dropped into water at the same speed behave differently: the water-repellent sphere drags a large air cavity behind it, while the wetting sphere enters with a small plop and no cavity (Duez et al., 2007). Aristoff and Bush (2009) measured the same cavity formation for small hydrophobic spheres. Spheres carrying a film of air on a superhydrophobic surface settle through water faster than uncoated spheres, a measured drag reduction of 5 to 15 percent (McHale et al., 2009).

In this framework the result is a direct reading of lattice connectivity. Same mass, same shape, same speed, same water. Where the lattice is severed at the surface by air, the coupling falls. Where the lattice wraps the body, full coupling holds.

## 7. One Medium, One Variable: Frequency and the Four Forces

### 7.1 One medium, four apparent forces

Sound travels faster through water than through air. Light travels slower through water than through vacuum. The same medium responds differently to different frequencies. That elementary observation holds the key to force unification. The water-matrix is one medium. Frequency is the single variable that decides how energy couples to it. What we classify as four fundamental forces are four regimes of frequency-dependent coupling through the same lattice. The medium does not change. The frequency changes. The coupling changes. The apparent force changes.

The strong force. At nuclear scales the lattice is compressed to femtometer spacings, the vibrational frequencies are enormous, and the coupling between energy and lattice is intense. That is the strong force. Confinement, the fact that quarks are never isolated, has a natural reading: at these frequencies the coupling is so intense that separating an excitation from the medium costs more energy than creating new excitations. The medium will not release what it holds.

The weak force. The weak force governs decay and transformation. In the frequency picture it operates where the coupling is loose enough to permit state change. The lattice at these frequencies does not grip. It permits transformation. Mass is the resistance of the lattice to acceleration at a given frequency: frequencies that couple tightly resist acceleration, and frequencies that couple loosely accelerate readily.

Electromagnetism. Electromagnetic radiation is frequency propagating through the water-matrix. The speed of light is set by the bulk modulus and density of the undisturbed lattice, as the speed of sound in any medium is set by its elasticity and density. Light travels slower through denser lattice. That is the same refractive index n(r) that produces the Schwarzschild metric. Electromagnetism is the propagation; gravity is the geometry the propagation creates.

Gravity. Gravity is the bulk coupling between frequency and lattice structure across all scales. Where the lattice is dense, coupling is intense. Where it is sparse, coupling is weak.

### 7.2 The hierarchy problem

Why does gravity appear so much weaker than the other forces? Gravity is not weak. It is the same coupling measured at lattice densities where the nodes are separated by astronomical distances rather than femtometers. The force is the same at every scale. The dilution by lattice sparseness creates the apparent weakness. Gravity is a lower-frequency strain of the same medium.

Hu et al. (2013) supplied the demonstration. They did not change the water. They changed the frequency response of the structure the waves passed through, and the gravitational coupling followed. Modify the frequency, modify the gravity. This is measured.

### 7.3 The spectrum of the lattice

The water-matrix supports a continuous spectrum, from nuclear-scale vibrations near $10^{23}$ Hz, through molecular vibrations near $10^{13}$ to $10^{14}$ Hz (including the 350 nm resonance at $8.56 \times 10^{14}$ Hz), down to gravitational-wave frequencies of $10^{-4}$ to $10^{4}$ Hz and tidal frequencies near $10^{-5}$ Hz. At every frequency the lattice responds according to its local density and bonding geometry. Nuclear physicists observe the

high-frequency end and call it the strong force. Particle physicists observe the transforming regime and call it the weak force. Optical and electrical engineers observe propagation and call it electromagnetism. Astronomers observe the bulk coupling and call it gravity. They are observing one medium at different frequencies. The classification into four forces is an artifact of the frequency at which the observation is made.

### 7.4 The graviton as a conjugate photon pair

Picture two people holding the ends of a heavy rope. At the same instant one whips the rope up and the other whips it down with equal force. The two waves meet in the middle and cancel; the rope can hang nearly still. Now grab the middle while the whip is traveling. The tension in your palm is enormous. Both people are still feeding real force into the line. The visible wave vanished. The physical push did not. Energy is conserved as tension in the medium.

The Electro-Gravi-Magnetic method of Storti and Desiato (2005) and Storti (2009) defines the graviton in exactly this way: a conjugate photon pair, two transverse electromagnetic waves 180 degrees out of phase, whose electric and magnetic fields sum to zero while the energy is conserved as stress in the medium. For wave 1 with fields $E_1$ and $B_1$ and wave 2 with $E_2 = -E_1$ and $B_2 = -B_1$, the sums E and B are zero while the stress-energy of the configuration remains. The radiative content vanishes. The mechanical content persists.

Two adjacent hydrogen bonds oscillating in antiphase make exactly this configuration, and the strong-weak anti-correlation of Section 3.1 is its measured physical basis: as one bond strengthens, its partner weakens. The electromagnetic faces of the paired motion cancel. The mechanical stress travels on through the network as a collective vibration. The graviton is not a separate particle. It is a collective antiphase mode of the hydrogen-bond network. This paper adopts the mathematics of the conjugate pair as the stress mode of the network and leaves the particle content of that mode uncommitted. The energy budget of the exchange is treated in the Cold Genesis framework (Arghirescu, 2015, 2024), which develops particle formation energies through vortex cascades in the sub-quantum medium.

This also answers why gravity is so much weaker than electromagnetism. Electromagnetic interactions come from single bond oscillations coupling directly to charge. Gravitational interactions come from the collective antiphase mode, which needs many bonds oscillating in step. The weakness of gravity is the difficulty of holding phase coherence across large regions of lattice, not a difference in the strength of the medium.

Within the Electro-Gravi-Magnetic method, cosmological parameters follow from the harmonic representation of fundamental particles: a Hubble constant near 67.08 km $s^{-1}$ $Mpc^{-1}$ and a background temperature near 2.7248 K, with a zero-point-field energy density threshold for accelerated expansion of $U < -2.52 \times 10^{-13}$ Pa that represents boundary physics rather than bulk vacuum energy (Storti, 2009). Storti made the Hubble constant prediction before the Planck data were released.

## 8. The Planetary Record: Tidal Dissipation

### 8.1 A prediction before the record

The order matters. The water-matrix model came first. From it followed a prediction: if water is the medium of gravitational coupling, water should take up gravitational forcing far more efficiently than

rock, and the tidal energy budgets of water worlds should show discrepancies the standard accounting cannot close from first principles. The tidal dissipation record was found afterward. It reads as the prediction said it would.

## 8.2 Earth

Earth's total tidal dissipation is about 3.7 terawatts, measured through lunar laser ranging and satellite altimetry. The oceans account for about 3.5 terawatts, 95 percent of the total. The solid Earth, 99.95 percent of the planet's mass, contributes about 0.2 terawatts (Egbert and Ray, 2000; Munk and Wunsch, 1998).

The oceans are about $1.4 \times 10^{21}$ kilograms, roughly 0.023 percent of Earth's mass. The liquid iron outer core alone is about $1.84 \times 10^{24}$ kilograms, some 1,300 times the mass of the oceans. The Moon's gravity acts on every kilogram of Earth according to its position, not its composition. Divide each share of the dissipation by its mass and one kilogram of ocean water does about 75,000 times the tidal work of one kilogram of solid Earth. The ratio of the totals alone is 3.5 to 0.2, about 17 to 1.

That attribution was never derived from first principles. It was a residual: the difference between a measured total and an estimated component. Zschau (1978) stated that the exact share of dissipation between the oceans and the solid Earth was unknown because the mechanisms in the rock were not understood. That honest uncertainty became, through the ordinary operation of institutional science, a permanent feature of the landscape.

Standard geophysics names real mechanisms for the disparity: near-resonance of ocean basins with tidal periods, bottom friction, internal waves breaking over rough topography, and the plain fluidity that allows large displacements. In the deep ocean the dissipation concentrates where internal tides break over ridges and rough seafloor (Egbert and Ray, 2000). This framework does not dispute those mechanisms. It proposes they are incomplete. The asymmetric hydrogen-bond network gives water a structural pathway for taking up and converting gravitational forcing that the rigid crystal lattices of rock do not possess. The 17 to 1 ratio is not only a consequence of mechanical freedom. It is the signature of preferential frequency-gravity coupling through the water-matrix.

## 8.3 Ganymede

Ganymede has a magnetic field, which requires a liquid iron dynamo. Bland, Showman and Tobie (2008) tested whether tidal heating could keep the core liquid and found no physically plausible scenario that produced enough heat to prevent the core from solidifying. The magnetic field that should not exist continues to exist. Ganymede has a deep subsurface ocean under constant forcing from Jupiter.

## 8.4 Enceladus

The south polar region of Enceladus radiates about 15.8 gigawatts (Howett et al., 2011), against an equilibrium tidal heating ceiling of about 1.1 gigawatts (Meyer and Wisdom, 2007). Silica grains carried out in the plume show hydrothermal activity in contact with a rocky seafloor at temperatures above about 90 degrees Celsius (Hsu et al., 2015). The ocean should have frozen solid long ago. It remains liquid and active at an order of magnitude beyond conventional prediction. Aygün and Čadek (2023) showed that treating the ocean with the full Navier-Stokes equations, in place of the Laplace tidal equations, changes the computed tidal heating and flow.

### 8.5 The pattern

Earth has the Moon. Ganymede has Jupiter. Enceladus has Saturn. In every case: water under strong tidal forcing from a massive partner, over a layered interior. In every case: an energy budget the standard framework cannot close from first principles. A 2025 review in Space Science Reviews states that the mechanisms producing heat through tidal friction in icy worlds remain poorly constrained (Tobie et al., 2025). Foundational work had already shown that fluid surface layers and convecting solid interiors cannot be treated as independent systems in tidal calculations (Běhounková et al., 2010). They are coupled. The coupling is not a correction. The coupling is the physics.

### 8.6 The resolution

Water couples to gravitational forcing with an efficiency other materials cannot approach because the asymmetric hydrogen-bond network provides a molecular mechanism for transmitting and converting tidal energy. The lattice acts as an amplifier: energy deposited at the surface propagates through the bond network into the interior. At Ganymede the ocean couples to interior heating efficiently enough to sustain the dynamo. At Enceladus the water-ice interface couples to tidal forcing to produce 15.8 gigawatts. At Earth the oceans carry 95 percent of the dissipation. In all three, water's role as the preferred medium of gravitational coupling closes the account.

## 9. The Electric Signature: Bent Ice Makes Charge

The lattice is not silent while it works. Bent, it charges.

### 9.1 The measured foundation

Wen and colleagues measured that ordinary ice produces electric charge when it is bent, with a flexoelectric coefficient of about 1.14 nanocoulombs per meter, comparable to the benchmark ceramics titanium dioxide and strontium titanate (Wen et al., 2025). Their samples were ice slabs about 2 millimeters thick, frozen between gold- or platinum-coated foil. Squeezing ice evenly makes no charge: its molecules point every which way and cancel. A bend stretches one side and squeezes the other. That uneven strain, the strain gradient, tips the balance and lines up charge.

In words: polarization equals the coefficient times the sharpness of the bend, $P = \mu \times G$. P is the bound charge per square meter at the surface, $\mu$ is $1.14 \times 10^{-9}$ coulombs per meter, and G is the strain gradient, which for a simple bend is one divided by the bend radius. A still bend holds its polarization but drives no current. Current flows only while the bend is changing, so bend, release and bend again gives alternating current at the rhythm of the bending. The same study found a ferroelectric surface layer a few tens of nanometers thick near −113 degrees Celsius and a reversal of the signal above about −25 degrees, which the authors trace to the surface beginning to premelt.

### 9.2 From bend to charge that leaves

A bend alone does not move charge from one particle to another. Its polarization is bound and lasts only while the bend lasts. Charge that leaves needs a carrier and something to strand it. Both are measured.

The carrier. Ice carries a thin liquid-like skin even below freezing, the quasi-liquid layer. Baker and Dash (1994) proposed that colliding ice particles pass some of this skin between them, and Mason and Dash

(2000) found that charge travels with the mass transferred between colliding ice surfaces. Like the water films on desert sand, the skin holds positive hydrogen ions and negative hydroxide ions that can move.

The stranding. High-speed imaging of water drops moving across a polymer surface showed charge, up to 4.1 nanocoulombs, appearing the moment water first touched the surface and again each time a stuck drop slipped free, and the charge stayed behind (Chen et al., 2025). Slide-electrification studies found the same pattern: water pulling back from a surface leaves charge on it (Stetten et al., 2019).

The proposed mechanism, in four steps. During contact, the bend polarizes the ice and sets up a field at the surface. Mobile ions in the liquid-like skin move to cancel that field. As the particles separate, the skin stretches and pulls back in stick-and-slip jumps. Each slip strands the gathered ions where they sit. The bend sets how much charge can move; the skin decides where it goes.

The proposed sign rule. Two ice surfaces pressed together bend as mirror images, so the bend alone cannot decide which particle ends up positive. The skin can. In Baker and Dash's picture, liquid flows from the thicker skin to the thinner one carrying negative charge, so the particle with the thicker skin ends positive. Riming warms graupel, and skin thickness changes steeply with temperature, so the charge should reverse at the temperature where the two skins are equally thick. Riming charge is known to reverse sign with temperature and liquid water content (Reynolds et al., 1957; Takahashi, 1978). The rule fits the relative growth rate theory, in which the faster-growing particle charges positively, because growth also changes the skin.

### 9.3 Lightning, worked by arithmetic

An ice crystal of radius 50 micrometers strikes a graupel pellet of radius 1 millimeter at 3 meters per second. Ice stiffness is 9.3 gigapascals. Hertz contact mechanics (Johnson, 1985) gives an effective radius of about 48 micrometers, a crystal mass of about $4.8 \times 10^{-10}$ kilograms, a compression of about 0.42 micrometers and a contact patch about 4.5 micrometers in radius.

The strain fades over about one contact radius, so the strain gradient is the strain divided by the contact radius. The stranded charge is at most the polarization times the patch area, which in words is pi times the coefficient times the strain times the contact radius. With strain held near 1 percent, because ice cracks or yields beyond that, the charge is $3.14 \times 1.14 \times 10^{-9} \times 0.01 \times 4.5 \times 10^{-6} \approx 1.6 \times 10^{-16}$ coulombs, about 0.16 femtocoulombs. At the full elastic strain of about 9 percent it is about 1.5 femtocoulombs. Laboratory ice collisions transfer charge in the femtocoulomb range (Pereyra and Avila, 2002).

A cloud-to-ground flash moves roughly 20 coulombs, three or four strokes of about 5 coulombs each. Let the collision rate in a 10-cubic-kilometer charging zone rise steadily from zero to $10^{14}$ per second over 15 minutes, matching radar studies of single-cell storms building for about 15 minutes before first flash (Courtier et al., 2019), then hold. At each step: the rate now, times the charge per collision (central case 0.36 femtocoulombs), times the step length, added to the total. Then shrink the step and watch the answer settle.

With one-minute steps the running total grows like this:

| After | Collisions per second during that minute | Total charge |
|---|---|---|
| 3 minutes | $1.3 \times 10^{13}$ | 0.43 coulombs |

| After | Collisions per second during that minute | Total charge |
|---|---|---|
| 6 minutes | $3.3 \times 10^{13}$ | 2.2 coulombs |
| 9 minutes | $5.3 \times 10^{13}$ | 5.2 coulombs |
| 12 minutes | $7.3 \times 10^{13}$ | 9.5 coulombs |
| 15 minutes | $9.3 \times 10^{13}$ | 15.1 coulombs |
| 18 minutes | $1.0 \times 10^{14}$ | 21.6 coulombs |

The total passes 20 coulombs during the eighteenth minute. Now shrink the step and watch the answer settle:

| Step size | First flash at |
|---|---|
| 5 minutes | 20.0 minutes |
| 1 minute | 18.0 minutes |
| 10 seconds | 17.0 minutes |
| 1 second | 16.8 minutes |

Each halving moves the answer less, and it settles near 17 minutes. Across the range, the first flash comes at about 28 minutes for 0.16 femtocoulombs and about 8 minutes for 1.5 femtocoulombs. Flexoelectric charging builds a first flash in 8 to 28 minutes, bracketing what radar observes. Mature storms flash every few seconds, which needs a larger charging zone or more charge per collision; this estimate addresses the first flash only.

### 9.4 The amorphous ice bilayer

The ice of space is mostly amorphous, laid down molecule by molecule on cold dust grains, in low- and high-density forms. Vapor frozen below about 30 K gives a dense form of about 1.1 to 1.15 grams per cubic centimeter that converts to the light form, about 0.94, between 38 and 68 K (Jenniskens and Blake, 1994).

Liquid water comes in the same two forms. Experiment has located a critical point between a low-density and a high-density liquid near 210 K and 1,000 bar (You et al., 2026), and structural analysis resolves the liquid into two dominant local arrangements (Li et al., 2026). The two densities are about 0.94 and 1.17 grams per cubic centimeter: the dense form is about 24 percent denser. A change from one form to the other changes size, and a change in size inside bonded layers makes a bend.

The test. Deposit a film of light amorphous ice, then a film of dense amorphous ice on top, on a thin silicon strip. Warm the pair through 38 to 68 K. The dense layer converts and grows by about 6 percent in length; the light layer does not; the pair curls. For a 0.5-micrometer converting layer on a 2-micrometer silicon strip, Stoney's formula (Stoney, 1909) gives a curl of $6 \times 9 \times 10^{9} \times 0.5 \times 10^{-6} \times 0.06 \div (160 \times 10^{9} \times (2 \times 10^{-6})^{2}) \approx 2{,}500$ per meter. The polarization is $1.14 \times 10^{-9} \times 2{,}500 \approx 2.9 \times 10^{-6}$ coulombs per square meter, about 0.29 nanocoulombs on a one-square-centimeter electrode. The film will

probably crack, since a 6 percent mismatch is hundreds of times the strain ice tolerates, and every crack tip is an extremely sharp strain gradient, so the signal may arrive in bursts.

Worked step by step. A change in density spreads over three directions, so the change in length is the cube root of the density ratio. For a dense form of 1.1, 1.1 ÷ 0.94 = 1.17, and the cube root of 1.17 is about 1.054: the layer grows about 5.4 percent in length. For 1.15 it grows about 7 percent. Take 6 percent. A free-standing pair of equal layers 1 micrometer thick would curl sharply, 1.5 × 0.06 ÷ 0.000001 = 90,000 per meter, but a film that thin cannot stand on its own at 15 K; it has to sit on a support, and the support resists the curl. The inputs to Stoney's formula are illustrative: ice stiffness of 9 gigapascals as a stand-in for the unmeasured amorphous value, and a silicon strip 2 micrometers thick with a stiffness of 160 gigapascals. The top of the fraction is 1,620, the bottom 0.64, and the curl about 2,500 per meter, about 35 times less than the free-standing case. Spread over a five-hour warming run of 18,000 seconds, the 0.29 nanocoulombs average a current of about 16 femtoamperes; an electrometer measuring the accumulated charge resolves far less than 0.29 nanocoulombs. Ice breaks at a stretch of only about 0.02 percent, a strength of about 1.5 megapascals divided by a stiffness of 9.3 gigapascals, so the smooth curl is an upper limit and the current should be recorded fast enough to see bursts, one per crack.

A pair of two light layers given the same warming never converts, so it should show nothing. The decisive control is a symmetric sandwich: light, dense, light. The middle converts and grows but is held equally from both sides, so the stack cannot curl. If the sandwich charges anyway, the flexoelectric reading fails. If the bilayer charges and the sandwich does not, the bend is the cause. Deposit the films in a vacuum cryostat with a gold electrode beneath the ice, since ice grown directly on platinum can carry its own built-in polarization (Su et al., 1998). Track the curl with a laser reflected off the tip of the strip, record charge with an electrometer, and check that the charge follows the measured curl through $P = \mu \times G$. Warming ice films also release trapped gas, so pressure is logged alongside. Comets and icy grains entering any planetary system pass through the same conversion window, so the bench test is also a test of a process on every icy body falling toward a star. Ice of that kind survives: the interstellar object 3I/ATLAS carried water ice beneath an irradiated crust about 15 to 20 meters thick after billions of years between the stars (Maggiolo et al., 2026; Cordiner et al., 2026), with a deuterium-to-hydrogen ratio of 0.98 percent measured by the James Webb Space Telescope (Salazar Manzano et al., 2026).

## 9.5 Tidal ice shelves

The Moon bends Antarctica's floating ice shelves twice a day. GPS on the McMurdo Ice Shelf recorded sideways motion up to 60 percent of the up-and-down tidal motion near the grounding line, explained by an elastic beam model of the bending (Rack et al., 2017). The energy is there to spend: the oceans dissipate about 3.5 terawatts of tidal energy, and shelf flexure is one of the places it goes. A 1-meter tide over a 3-kilometer bend gives a peak strain gradient of about $2.2 \times 10^{-7}$ per meter, building over a quarter of the 12.42-hour tide, about 11,200 seconds, so it changes by about $2.0 \times 10^{-11}$ per meter each second. The current is the coefficient times the rate of change: $1.14 \times 10^{-9} \times 2.0 \times 10^{-11} \approx 2.3 \times 10^{-20}$ amperes per square meter, only about 23 femtoamperes across a square kilometer of smooth ice. The measurable signal must come from where bending concentrates: crack tips, crevasses and the grounding line. The prediction is a voltage oscillating at 12.42 hours, much stronger across a crevasse than on smooth ice, after subtracting the field induced by tidal seawater moving through Earth's magnetic field, which satellites detect (Tyler et al., 2003).

How to test it. Place electrode pairs across a crevasse near a grounding line, a second set on smooth ice away from cracks, and a reference pair farther off, and record for several weeks alongside weather and temperature. The field induced by tidal seawater is spread over large distances, so it reads nearly the same on neighboring electrode pairs, and comparing the crevasse pair with the smooth pair cancels most of it. Crevasses also open and close with the tide, changing electrode contact in the snow, so contact resistance is logged too.

### 9.6 Electricity from water's surfaces

Engineers now draw electricity and chemistry straight from water's surfaces and interfaces, with no fuel and no moving parts. Every entry is a laboratory measurement.

| Year | Measured result | Source |
|---|---|---|
| 2026 | Continuous electricity from evaporating saltwater over silicon nanopillars: 1 V and 0.25 W per square meter, with heat and light steering charge at the liquid-solid interface | Anwar and Tagliabue, 2026 |
| 2025 | Water squeezed into channels a few molecules thick: an in-plane dielectric constant near 1,000 and conductivity far above bulk water | Wang et al., 2025 |
| 2025 | Oppositely charged water microdroplets spark when they come close, and the sparks form organic molecules from the surrounding gases | Meng, Xia, Xu and Zare, 2025 |
| 2023 | Light evaporates water at the air interface without heating it, peaking in green light, by cleaving clusters of molecules off the surface; the finding was put through 14 separate tests | Tu et al., 2023 |
| 2020 | Water condensing as microdroplets on cold silicon, glass, plastic and metal makes hydrogen peroxide on its own, with no catalyst or applied voltage | Lee et al., 2020 |
| 2020 | One 0.1 mL drop falling 15 cm gives over 140 V and lights 100 small LEDs | Xu et al., 2020 |
| 2018 | Water a few molecular layers thick has a perpendicular dielectric constant of about 2, against about 80 for bulk water | Fumagalli et al., 2018 |

### 9.7 The strain gradient is the common currency

Every result in this section comes from one quantity: the strain gradient, how sharply stretching changes from place to place. In bent ice it lines up charge. At a crack tip it peaks. In a collision it sets the stranded charge. At tidal frequencies it bends the ice shelves of Antarctica.

The same quantity sits at the heart of gravity. What a freely falling observer actually measures is tidal stretching, the difference in pull across a body, and that is what curvature means physically. The strain gradient that makes charge in ice and the strain gradient general relativity calls curvature are the same operation on the same medium. Where the lattice strains, it charges. Where mass strains the lattice, it gravitates. The electric signature and the metric are two measurements of one deformation.

## 10. Water in Living Matter

By molecule count, not by mass, a human being is roughly 99 percent water. Mass hides this, because water molecules are featherweights beside proteins. Count the molecules and nine hundred ninety in every thousand are water. The proteins, membranes and DNA are minority structures suspended in, and shaped by, the lattice this paper describes. This section carries the strong-weak rule into living matter, where its consequences can be tested on a bench.

### 10.1 Hydration solids

Hygroscopic biological matter is everywhere. Bacterial spores, pollen, fungal walls and plant tissues all exchange water with their surroundings and change size and stiffness with humidity, despite entirely different chemistry. Harrellson and colleagues showed that this shared behavior comes from one mechanism: the hydration force, a short-range repulsive force that dominates when pores shrink to nanometers (Harrellson et al., 2023). In the cortex of Bacillus subtilis spores, whose pores are about 4 nm across, water moves orders of magnitude slower than any diffusion model predicts. They named matter governed this way a hydration solid.

In a 4 nm pore the hydration force fields from opposite walls overlap across the whole channel. Every water molecule in transit feels both walls at once. Now add the strong-weak rule. Water molecules do not enter the pore as symmetric, freely turning objects. Each arrives already committed: one hydrogen to a strong bond, the other to a weak one. To satisfy the left wall it must point one hydrogen there; to satisfy the right wall, the other. It cannot present equal bonding to both. The molecule is structurally frustrated.

The frustration does not merely add to the hydration barrier. It couples with it. The hydration force builds the barrier landscape; the bond asymmetry ensures that the molecule crossing that landscape is poorly equipped to cross it. Because the anti-correlation is modulated by thermal motion on sub-picosecond timescales, there are brief windows when the asymmetry relaxes. Those windows are the main opportunities for passage. Water transport through hydration solids is then stochastic and thermally gated rather than continuously slow: rare, intermittent transit events when a fluctuation lets a molecule satisfy both walls. The hygroelastic transition, the jamming-like stiffening of spores at short timescales, may be tuned in part by the same thermal modulation, so conditions that alter it, such as temperature, ionic environment or isotopic composition, should shift the timescale of the transition.

### 10.2 The hydrated helix

The DNA double helix keeps its B form only when it is wet. Dry it and the helix drives into other shapes or disorder. Crystallography resolves an ordered chain of water molecules in the minor groove, the spine of hydration. Chiral sum-frequency spectroscopy shows that DNA confers its handedness on the first shell of water, a structured phase distinct from bulk solvent (McDermott et al., 2017; Perets and Yan,

2017; Perets et al., 2024), and a drug binding to DNA disrupts that chiral water (Santiago et al., 2025). Nuclear magnetic resonance measures how long it stays: spine water in the minor groove resides about 1 nanosecond at 4 °C and 10 to 15 nanoseconds at the lowest temperatures measured, roughly ten times longer than water in the major groove (Halle and Denisov, 1998).

The minor groove meets both conditions of the hydration solid framework. It is a channel of nanometer width bounded by sugar-phosphate backbones, whose anionic phosphate oxygens are among the strongest hydrogen-bond acceptors in biology, and floored by base-edge oxygens and ring nitrogens of weaker and geometrically different character. The first proposal is that the DNA groove is a hydration solid geometry.

The second is that the strong-weak rule helps order it. Spine water resides about a nanosecond, some three orders of magnitude longer than the 500-femtosecond refresh of the anti-correlation, so the asymmetry is a standing property of each resident molecule. A first-shell molecule donates its two bonds to unequal acceptors: the strong, anionic phosphate oxygens and the weaker base edges. Where the strong bond finds the stronger acceptor and the weak bond the weaker, both donors are matched, and that biases the stable occupation of hydration positions alongside electrostatics, geometry and counterions. A mismatched molecule can only rearrange by re-randomizing the anti-correlation itself, a step added to the translations and rotations by which shell water is usually modeled to exchange.

## 10.3 The electrical hydrogen bond

The hydrogen bond is an electrical structure. It shares electrons (Isaacs et al., 1999). It moves about a fiftieth of an electron's charge per bond, and pH shifts that charge flow by measured percentages (Flór et al., 2024). Charge travels along chains of hydrogen bonds: a proton's charge moves by hopping as covalent and hydrogen bonds exchange partners, so the charge travels rather than the proton's mass, and proton jumps of about 0.5 to 0.7 ångström have been observed directly, correlated with each other (Popov et al., 2023). Femtosecond spectroscopy finds the proton shuttling between neighboring oxygens in under 100 femtoseconds, at least 15 water molecules taking part in moving one proton's charge, and proton transfer between an acid and a base running through a hydrogen-bonded water wire of 2 to 4 molecules (Bakker group, AMOLF). In the Grotthuss mechanism the Eigen form, $H_9O_4^+$, and the Zundel form, $H_5O_2^+$, interconvert, and net charge transport can outrun any single proton.

DNA is electrically active, and its water switches it on. Charge travels through DNA 100 base pairs long, 34 nanometers, and a single mismatched base pair cuts the signal roughly in half, a ratio of 2.3 ± 0.4; the authors attribute the transport to the stacked bases (Slinker et al., 2011). DNA molecules 414 base pairs long between gold electrodes measured about 10 teraohms at 30 percent relative humidity and about 250 megohms at 80 to 90 percent, a drop of some 40,000 times that reversed on drying; the authors could not separate the contributions of electrons, protons and ions (Tuukkanen et al., 2005). The third proposal is that the asymmetric hydration shell is part of DNA's electrical pathway. Resident molecules, each holding one strong and one weak bond in fixed relation to the groove, form ordered hydrogen-bond chains along the helix, and ordered chains are what charge moves along in water. A mismatch or lesion that alters the groove alters the shell, and with it the pathway. The electrical signature of damaged DNA would then be read partly through its water, a connection with direct bearing on oncology. Relationships between cellular water state, membrane potential and tissue mechanics have

been documented without a molecular mechanism (Cone, 1971; Holmes, 2026). The molecular layer described here is where that chain begins: molecule to shell, shell to chromatin, chromatin to cell.

### 10.4 Carbon scaffolding

Carbon-12, about 98.9 percent of all carbon, has 6 protons, 6 neutrons and 6 electrons. Carbon closes itself into six-member rings in benzene and graphene. Ice is built from six-member rings of water. Three amino acids, phenylalanine, tyrosine and tryptophan, carry six-carbon rings. Every level of this scaffolding bonds to water.

Neutron crystallography sees hydrogen, so it shows which way water points. Around DNA, neutron data give the orientation of the water touching the helix (Harp et al., 2021). In the protein crambin, ultrahigh-resolution neutron work located 299 of the protein's 315 hydrogens directly and oriented the water in the first and second shells around it (Chen et al., 2012). An Antarctic bacterium, Marinomonas primoryensis, makes an antifreeze protein that anchors ice-like clathrate water to its own surface, matching the planes of real ice in three dimensions, and uses it to grab ice (Garnham, Campbell and Davies, 2011). A fish-type antifreeze protein folds around an interior network of more than 400 water molecules; its helices barely touch, and water holds it together from the inside (Sun et al., 2014). A snow mold fungus carries a bound-water network across its ice-binding face, and the versions with more network work better (Khan et al., 2021). Pure water can stay liquid down to about −40 °C; with the bacterium Pseudomonas syringae present it freezes at about −2 °C (Maki et al., 1974), and the bacterium's ice-nucleating proteins order the water beside them (Pandey et al., 2016). In the protein BRD4 a conserved water network forms the binding site itself (Piticchio et al., 2025). In the photosynthetic FMO protein, one of the carbon-ring pigments is held to the protein by a single water molecule (Tronrud et al., 2009).

One level down, water's hydrogen points at a carbon ring's cloud of electrons, and rotational spectra show one or two water molecules bridging benzene rings (Steber et al., 2025). Under a graphene sheet, the first layer of water on mica is ice-like at room temperature (Xu, Cao and Heath, 2010). Water gives its hydrogen to the nitrogen of an imidazole ring in a nearly straight line, read by microwave spectroscopy across several isotope versions (Gougoula et al., 2022), to ammonia (Herbine and Dyke, 1985), and to the nitrogen gas of the air: the nitrogen-water complex is nearly linear, with the water's hydrogen 2.42 ångströms from the nitrogen, measured across seven isotopic species (Leung et al., 1989). In mixtures of nitrogen and water vapor, the measured absorption near 4 micrometers, the region of nitrogen's own fundamental band, runs up to two orders of magnitude above the standard continuum model (Baranov, 2011). The air itself is bonding to water. The shape of the water changes with what it holds: hexagons on flat carbon, pentagons in the fish protein, zigzags on the fungal protein. At every level, from the code down to the air, the bond uses the same four points.

Collagen, the body's principal structural protein, is built the same way. Crystallography of a collagen peptide resolves a cylinder of hydration around each triple helix: water in four-, five- and six-membered rings anchored to backbone carbonyls and hydroxyproline (Bella, Brodsky and Berman, 1995). The helices do not touch; water carries the force between them. Direct measurements between helices in native and reconstituted fibers found exponential hydration forces (Leikin, Rau and Parsegian, 1994). Raman spectra taken on the same samples show the hydrogen-bonding structure of the water changing continuously with the separation (Leikin et al., 1997), and the repulsion at surface separations of 0 to 8

ångströms comes from the cost of perturbing the hydrogen-bonded network of the solvent (Kuznetsova et al., 1997). Swap $H_2O$ for $D_2O$, whose hydrogen bonds are about 10 percent stronger, and collagen assembles ten times faster, into thinner fibrils and a network four times softer (Giubertoni et al., 2024). In bone, solid-state NMR finds a highly ordered layer of water between the mineral and the collagen (Wilson et al., 2005). The protein frame is the loom; the water is the weave.

Raman micro-spectroscopy of single living cells finds a small, consistent population, about 3 percent, of non-bulk water with a weakened hydrogen-bonded network and a more disordered tetrahedral structure, about one molecular layer, 2.6 ångströms, around the proteins (Lang et al., 2024). In this framework that is the scaffold's engine observed mid-cycle: a network defined by continuous strong-weak exchange reads as locally disordered at any instant. Static disorder and dynamic order are the same system seen at different exposure times.

### 10.5 The networks of life

In 2026 Meng and colleagues compared how physical networks branch across living systems, using high-resolution three-dimensional scans of human and fruit-fly neurons, human blood vessels, tropical trees, corals and the plant Arabidopsis (Meng et al., 2026). A century of wiring theory says networks branch to minimize running cost. The mathematics of minimal surfaces, developed by string theorists in the 1980s, says otherwise. The scans favored surface minimization across all six network types. It predicted three-way, four-way and higher junctions the older theory cannot, and thin perpendicular sprouts. In the human brain, 98 percent of those sprouts end in synapses.

Why would neurons, trees and corals, with no communication across kingdoms, obey the same geometry? If every city on Earth, built in isolation, were laid out on the same street grid, you would not conclude they invented the same idea. You would conclude they were built on the same terrain. Living tissue is mostly water by molecule count, its proteins fold by hydrogen bonding into that network, and its membranes organize against it. The minimal-surface geometry is the geometry of the water lattice that every one of those networks grows inside. Life does not fight physical law. It uses the geometry of the substrate it is made of.

### 10.6 Proposed experiments

Each test uses existing methods. In each, the mass-dependent isotope effect is the null hypothesis.

Isotopic substitution in spores. Compare water transport in Bacillus subtilis spores in $H_2O$, in $D_2O$ and in a controlled mixture, using the nanomechanical cantilever method of Harrellson et al.: spore-coated cantilevers given photothermal pulses, with the deflection reporting water-exchange timescales at controlled relative humidity. Prediction: $D_2O$ moves through the cortex pores slower than $H_2O$ by a margin beyond what the mass difference alone predicts. The size of the excess measures the asymmetry's share of the barrier.

Isotopic substitution in DNA. Deuterium strengthens hydrogen bonds and alters the anti-correlation statistics, which is the operating principle of the Gunkel et al. measurements themselves. If the asymmetry helps order the shell, $D_2O$ substitution changes first-shell ordering and exchange by more than the mass effect on diffusion, detectable by chiral sum-frequency spectroscopy, which isolates the first hydration shell (Perets et al., 2024), or by water-exchange timing on DNA films and DNA-coated cantilevers.

Counterions and temperature. Weakly hydrated ions restructure confined hydrogen-bond networks and speed water through nanochannels (Bi et al., 2026), so network statistics can be dialed under confinement. Shell observables should shift systematically across the alkali series, which grades in hydration character, and with temperature, which changes the anti-correlation lifetime. Observables that track only ion charge and bulk viscosity disfavor the mechanism.

Sequence dependence. AT-rich sequences, with narrow minor grooves presenting a coherent acceptor pattern, offer a sterner test than GC-rich sequences with wider grooves and an exocyclic amino group. Chiral sum-frequency or crystallographic water-occupancy comparisons across defined sequences would detect the dependence.

Hydration and charge transport. Measure charge transport through matched and mismatched DNA, as in Slinker et al. (2011), and conductance across relative humidity, as in Tuukkanen et al. (2005), in $H_2O$ and in $D_2O$. A change in conduction in $D_2O$ beyond the mass effect, or a mismatch effect that changes with hydration, is the signature of the shell pathway.

## 11. Strings Are Hydrogen Bonds

### 11.1 The identification

String theory proposes that the fundamental constituents of nature are one-dimensional vibrating strings whose vibrational modes set particle properties. Its mathematics closes only with six extra spatial dimensions, rolled up so tightly at every point that no instrument can see them, in a shape called a Calabi-Yau manifold. Enumerating the possible shapes yields a landscape of about $10^{500}$ candidate universes.

Read that summary again with the water molecule in mind. A pervasive network of one-dimensional connections between nodes, each connection vibrating. Vibrations whose allowed patterns determine observable properties. Six hidden degrees of freedom riding at every point.

The strings are hydrogen bonds. Each bond is a one-dimensional connection between two lattice nodes. Each bond vibrates, breaking and re-forming about a trillion times per second while the strong-weak rule holds. The vibrational spectrum of these bonds under varying density and strain produces the spectrum string theory was built to reproduce. At nuclear density the modes are the strong-force regime. At molecular density they are chemistry and electromagnetism. At cosmic density they are gravitational coupling.

### 11.2 The six dimensions

The six compactified dimensions are the six internal degrees of freedom of the water molecule at each node. Count them.

One, two, three: rotation. The tetrahedral molecule aims its four docking sites by turning about three independent axes.

Four: the strong-weak toggle. Each donated bond is strong or weak, a strict two-state switch flipping under the seesaw rule. A discrete two-state degree of freedom maps onto the spin one-half representation of SU(2) symmetry.

Five and six: vibration. The oxygen-hydrogen stretch, breathing like a spring, and the hydrogen-oxygen-hydrogen bend, opening and closing like a hinge.

Three rotations, one switch, two vibrations: six degrees of freedom at every node, everywhere, always. They are compactified because they are internal to the node. They are not large-scale spatial dimensions, but they decide the properties observed at the node.

The Calabi-Yau manifold corresponds to the $sp^3$ hybridization geometry of the water molecule, the tetrahedral bonding architecture mapped into an abstract space. It is not hidden geometry at the Planck scale. It is the bonding geometry of every water molecule, measured in every chemistry laboratory, present at every node of the lattice. The shape drawn at the summit of abstraction is the shape in a teacup.

### 11.3 The landscape

Different strain regimes of the lattice produce different effective physics. The landscape of about $10^{500}$ abstract configurations reduces to the space of physically realizable strain states of the water-matrix, from the sparse interstellar medium to the extreme compression at a gravastar boundary. The gravastar shell occupies the far end of that landscape, where the vibrational spectrum produces the ultra-stiff equation of state $p = \varepsilon$ that the gravastar requires (Section 18).

### 11.4 Five dimensions and SU(2)

Gold and colleagues constructed all gauged curvature-squared supergravity invariants in five dimensions within an SU(2) gauge structure (Gold et al., 2023). The water-matrix carries the same SU(2) structure, the two-state character of each bond mapping onto spin one-half. The five dimensions acquire a physical reading: three of space, the radial strain dimension, and the frequency dimension at 350 nm. The curvature-squared corrections correspond to the higher-order refractive terms predicted as deviations from the Schwarzschild metric at the level of about two microarcseconds (Section 25).

### 11.5 Two manifolds, one object

String theory is not wrong on this reading. It is right about the structure and wrong about the address. It describes a real, vibrating, sixfold, networked medium, and it hid that medium inside imaginary curled geometry because it inherited the assumption that the medium of experiment is empty.

The manifold of general relativity is the graded refractive index of the strained lattice (Section 5). The manifold of string theory is the bonding geometry of the same lattice and its vibrational spectrum. The two formalisms are coherent with each other because both describe one substance. A manifold does not stop being a manifold when its density drops; the lattice can thin to a single line of molecules and still carry its node geometry. The biological networks of Section 10.5 following string theory's minimal-surface mathematics is the same identification seen from the living side. String theory, developed over decades as abstract mathematics, and the water-matrix, developed from empirical observation, meet without either having been built with knowledge of the other.

## 12. The Double Slit and the Room That Cannot Be Emptied

### 12.1 The experiment

Cut two narrow slits side by side in a barrier. Behind it, place a screen that records impacts. Fire single particles at it, one at a time. If particles were bullets you would get two piles, one behind each slit. Instead, over thousands of firings, the screen fills with stripes: a band of hits, a gap, another band. Stripes are what waves do when two sets of ripples overlap. Physics answered with superposition: the particle in flight is a spread of possibilities across both paths until detection snaps it to one point. A century of argument about observers, collapse and parallel worlds rests on those stripes.

The double slit began as a water experiment. Thomas Young worked out interference from tides and water waves first and showed it in a ripple tank before carrying the same rule over to light (Young, 1802, 1807; Mollon, 2002).

Now ask the question every controlled experiment demands. What was in the room?

### 12.2 The vacuum record

Every one of those experiments ran inside a vacuum chamber built to hold nothing. Attach a residual gas analyzer, a small mass spectrometer that weighs what is left, and the answer is the same at every laboratory that has checked. In an unbaked stainless steel chamber the dominant residual peak is mass 18, water. Over a standard 50-hour observation, the outgassing of stainless steel and aluminum chambers was more than 85 percent water, and electropolishing gave no significant reduction against a simple detergent wash (Dylla, Manos and LaMarche, 1993). For an unbaked accelerator system, every species in a residual gas scan is normalized to the dominant peak, mass 18 (Vacuum acceptance tests, 2020). After a 150 °C bakeout and five days of pumping at $2 \times 10^{-8}$ mbar, water was still the main component of the residual gas in a plasma laboratory (D-Mag, 2023). A 2024 review states it plainly: for many processes in vacuum the presence of water is both undesirable and unavoidable (Gorkhover, 2024).

The flying molecules are not the main story. The walls are. A steel surface that has seen air carries water tens of monolayers deep, on the order of $10^{16}$ molecules per square centimeter, roughly a gram of water on the walls of a one-cubic-meter chamber, against about $3 \times 10^{9}$ molecules per cubic centimeter in flight at $10^{-7}$ Torr. A water molecule sits on room-temperature stainless steel for about a week, pops loose, crosses the chamber without striking another molecule, and lands on another wall (Chiggiato, 2020). The walls hold about a million times more water than the volume, and the two populations exchange continuously.

Every countermeasure manages the water. None removes it. A 200 °C bake strips several monolayers and leaves water as background. Cryopumps condense water onto cold panels, where it stays in the chamber until the panels warm and release it. Steel fired at 950 to 1,050 °C before assembly picks up water again the moment it meets air. The outgassing never falls to zero; the rate decays with pumping time but its integral cannot run to infinity (Chiggiato, 2020). In the 1.9 K arcs of the Large Hadron Collider, water is never pumped out at all; it is frozen onto the cold bore and stays there, which is why the listed residual gas of the beam vacuum names hydrogen, methane, carbon monoxide and carbon dioxide but not water (Gröbner, 1997; Evans and Bryant, 2008).

Put the vacuum record beside Section 2.4. Every vacuum chamber on Earth holds a standing water population that cannot be removed. Water molecules attract at any distance and, wherever they coexist, form one stretched network. The rooms physics calls empty contain a connected, structured, electrically active lattice lining every surface and stretched across the volume. Every quantum experiment ever performed on Earth was performed inside water.

### 12.3 The bookkeeping of the vacuum

The water dominance is a raw readout, not a model. One residual gas analyzer log printed in the Stanford Research Systems application note on vacuum diagnosis reads:

| Species | Mass (amu) | Partial pressure (Torr) |
|---|---|---|
| Hydrogen, $H_2$ | 2 | $7.1 \times 10^{-8}$ |
| Water, $H_2O$ | 18 | $1.4 \times 10^{-5}$ |
| Nitrogen, $N_2$ | 28 | $4.6 \times 10^{-10}$ |
| Oxygen, $O_2$ | 32 | $3.4 \times 10^{-11}$ |
| Carbon dioxide, $CO_2$ | 44 | $1.6 \times 10^{-12}$ |

The mass-18 peak stands more than two orders of magnitude above every other species. At $10^{-7}$ Torr the residual gas is 85 to 90 percent water (Kurt J. Lesker Company; Poseidon Scientific). For scale, ordinary air holds about $10^{20}$ molecules per cubic centimeter and a typical high vacuum about $10^{10}$.

The outgassing has a bookkeeping of its own. For unbaked metals the water outgassing rate falls only as one over the pumping time: $q(H_2O) \approx 3 \times 10^{-9}$ divided by the hours of pumping, in mbar liters per second per square centimeter (Dylla, Manos and LaMarche, 1993). After 10 hours that is $3 \times 10^{-10}$, about $7 \times 10^{9}$ water molecules leaving every square centimeter every second. Edwards measured $2 \times 10^{-10}$ Torr liters per second per square centimeter at 10 hours and found the value held for all metals used to build vacuum chambers (Edwards, 1977). Across stainless steels whose surface roughness differed by more than two orders of magnitude, the outgassing rates differed by only a factor of 2.8 (Dylla, Manos and LaMarche, 1993). The rate of an unbaked surface is not a property of the material; it depends on how long it has been pumped, and the water inventory recharges at every venting to air (Chiggiato, 2020). The pump only sets a balance point. Outgassing equals pumping speed times pressure, $Q = S \times P$, so the partial pressure of water is a direct readout of its inflow. Seal the chamber and the pressure climbs at the rate the walls release.

Water's desorption energy on stainless steel and aluminum, 19 to 23 kilocalories per mole, falls inside the 15 to 25 kilocalorie band the vacuum literature identifies as the range that dominates outgassing (A Review of Outgassing and Methods for its Reduction). The binding energy is why the population stands. Bake a chamber above 100 °C and a water molecule's stay on the surface drops to about a minute; cool a metal surface to 77 K and it pumps water and nothing else (Baglin, CERN Accelerator School).

When the water is driven down, hydrogen dissolved in the steel takes over, and it too never reaches zero. A stainless steel chamber baked at 250 °C for 380 hours outgassed $2.86 \times 10^{-13}$ mbar liters per

second per square centimeter; a further 140 hours at 350 °C brought it to $5.7 \times 10^{-14}$ (Avdiaj and Erjavec, 2012). Each escalation of effort buys about one decade, and the curve flattens while staying finite.

Every laboratory that looks reports the same thing. The main residual of an unbaked stainless steel system is water (Khan et al., 2017). While an unbaked chamber is pumped, water vapor is the predominant desorbing gas (Akaishi et al., 1999). Any charged particle crossing such a chamber meets water first, because water is nearly the whole gas: electron beams, ion beams, trapped particles and plasmas meet water-group species, whose OH and $H^+$ fragments register in detectors.

## 12.4 Inside the colliders

The largest machines in physics treat water the same way. The beam pipe of the Large Hadron Collider is 54 km of ultrahigh vacuum, and 48 km of it sits at 1.9 K, where the pipe wall itself freezes gas out of the volume. Its beam vacuum is designed for about $10^7$ molecules per cubic centimeter (Bregliozzi, 2023).

| Part | Length | Temperature | How gas is removed |
|---|---|---|---|
| Arcs, cold bore | 48 km | 1.9 K | The pipe wall is a cryopump: gas freezes onto it |
| Beam screen inside the cold bore | 48 km | 5 to 20 K | Intercepts heat; perforated so gas passes to the 1.9 K wall |
| Long straight sections | about 6 km | Room temperature | Baked, then pumped by a titanium-zirconium-vanadium getter coating and ion pumps |
| Magnet insulation vacuum | 24 km, 640 cubic meters | Cryogenic | Cryopumping to the $10^{-6}$ mbar range |

Source: LHC beam and insulation vacuum systems, AVS 2008. The cold bore is 49 mm across inside, and the beam screen was made partly open so that gas released by the beam could be pumped permanently on the 1.9 K surface (Gröbner, 1997).

Before each cool-down the cold sections are pumped for weeks: during the 2013 to 2014 shutdown every cryogenic vacuum system was evacuated for at least five weeks to remove residual gas, mainly water vapor (Baglin et al., 2014). In the cold arcs water is frozen, not removed: $CH_4$, $H_2O$, CO and $CO_2$ are held first on the 5 to 20 K beam screen and then on the 1.9 K cold bore (Bregliozzi, 2023). The beam knocks frozen gas back off the walls: electron-stimulated desorption can be 100 times stronger than photon desorption, and more than 100 monolayers of gas are available on the surfaces (Baglin et al., 2002). In the warm sections, the getter-coated pipes are held at 120 °C during bakeout to keep them from absorbing water (Bregliozzi et al., 2008). About 20 vacuum sectors a year must be baked after technical stops, at about 300,000 euros a year, and water desorption is the main obstacle to reaching ultrahigh vacuum quickly (Ortino, Politecnico di Milano).

In 2017 air leaked into one cell, 16L2, during cool-down and froze onto the 20 K beam screen. CERN's account is that frozen particles detached, fell into the beam and turned to gas, causing losses and

instabilities (CERN, 2017). There were more than 60 premature beam dumps, and the machine ran with about 25 percent fewer bunches than nominal for most of the year (Mether et al., 2017). A 2023 CERN slide of the site marks the warmer 50 K surface as covered with $H_2O$ (Mether, 2023).

The protons do travel through gas. The vacuum is designed so that a proton strikes a gas nucleus no more than about once per 100 hours of circulation: $1/\tau = \sigma c n$, where $\sigma$ is the scattering cross section, c the speed of light and n the gas density (Gröbner, 1997). Heavier molecules scatter protons more, so less of them is allowed:

| Gas | Cross section at 7 TeV ($cm^2$) | Density allowed for 100 hours (per $m^3$) |
|---|---|---|
| $H_2$ | $9.5 \times 10^{-26}$ | $9.8 \times 10^{14}$ |
| He | $1.26 \times 10^{-25}$ | $7.4 \times 10^{14}$ |
| $CH_4$ | $5.66 \times 10^{-25}$ | $1.6 \times 10^{14}$ |
| $H_2O$ | $5.65 \times 10^{-25}$ | $1.6 \times 10^{14}$ |
| CO | $8.54 \times 10^{-25}$ | $1.1 \times 10^{14}$ |

Source: LHC Machine, table 5.1 (Evans and Bryant, 2008). For the High-Luminosity upgrade, which doubles the current, the allowed water density is halved to $9.6 \times 10^{13}$ per cubic meter (CERN, 2020). A proton that strikes a gas nucleus sprays secondaries into the superconducting magnets, and the design allows about 0.1 W per meter of this heating (Gröbner, 1997).

At the detectors, collisions with the gas are a measured signal. ATLAS reports that inelastic beam-gas collisions within a few hundred meters of the detector are the dominant source of beam background; when gas was injected locally into the beam vacuum in dedicated tests, the backgrounds rose and fell with the local pressure, and the rate depends on the density and the molecular composition of the residual gas (ATLAS Collaboration, 2024). LHCb injects gas on purpose. Its SMOG2 system holds gas in a 20 cm storage cell 34 cm from the collision point and uses the beam-gas collisions as a fixed-target experiment; helium, neon, argon and hydrogen have been injected, and deuterium, nitrogen, oxygen, krypton and xenon are being studied (LHCb SMOG2, 2024). Water is on neither list.

Japan's SuperKEKB collider reports water directly in the gas its beams travel through. The 3,016 m ring is pumped mainly by getter strips near 100 nPa (Belle II, 2023). During beam operation in 2016 the main residual gases were hydrogen, carbon monoxide, methane, water and carbon dioxide, and because the beam pipes were not baked in the tunnel, water vapor remained in them (Suetsugu et al., 2016). Two residual gas analyzers now measure the composition in the ring, and beam-gas scattering remains the largest background in the positron ring (Nakayama, 2021).

## 12.5 The cost of fighting water

Gravitational-wave observatories measure their residual water because they pay to remove it. The water removed from one 2 km LIGO beam tube module during pump-down and bakeout was close to $5 \times 10^5$ torr liters, 25 moles, about 450 grams, from an initial surface coverage of about 190 monolayers (LIGO T990186, 1999). The beam tube modules were baked at 160 °C for one month to reduce water vapor, and later exposures to air compromised the performance again (LIGO E1600073, 2016). Water

vapor ingested from 2008 to 2012 raised the outgassing of the Livingston Y tube past its limit, and the midstation analyzer recorded water at $1.5 \times 10^{-10}$ torr (LIGO T1500202, 2015). LIGO's 50 km of welded beam tube at about $10^{-9}$ torr carried a budget of about 40 million dollars in 1997, and passive 80 K cryotraps pump the water released by detector parts (Zucker, LIGO G1900137, 2019). Besides the cost of steel, water outgassing is a main concern, and bakeouts near 200 °C are very costly in equipment, labor and time (LIGO G2302149, 2023). About 34 percent of the cost of the planned Cosmic Explorer is in its ultrahigh vacuum system, and the standard way to remove water is to bake the walls (Cosmic Explorer Horizon Study, 2021). For the Einstein Telescope, the beam pipe is estimated at about 440 million euros and the vacuum system at about one third of the total budget, for 120 km of 1 m pipe, with a dry nitrogen purging study to reduce water readsorption (Scarcia, CERN Einstein Telescope vacuum group, 2025).

The observatories spend tens to hundreds of millions of dollars on the water and measure it by residual gas analysis. The matter-wave interferometers in the record report total pressure only.

## 12.6 The largest superposition

In 2026 a University of Vienna team interfered sodium clusters heavier than 170,000 daltons, more than 7,000 atoms each and heavier than most proteins, in a Talbot-Lau interferometer of three ultraviolet standing-wave gratings 0.983 meters apart, at a chamber pressure of $9 \times 10^{-9}$ mbar (Pedalino et al., 2026). By the authors' own comparison the clusters, about 8 nm across, were more massive than immunoglobulin G at 150 kDa. Sodium was evaporated at 650 to 700 K into an argon-helium mixture at 77 K below 1 mbar; the clusters flew at 120 to 170 m/s, with de Broglie wavelengths of 10 to 22 femtometers and a longitudinal coherence length of 160 to 350 femtometers, and passed three differential pumping stages through a 5 mm aperture. Fringe visibilities were 0.08 to 0.10 at grating powers of 62, 15.2 and 68 mW. The authors' next target approaches the megadalton range of small viruses. The paper reports the total pressure with full precision. No instrument in the apparatus measured the composition of the residual gas. The partial pressure of water appears in no error budget, no model and no analysis. Nobody lied and nobody was careless. The omission is inherited from a century-old habit of describing high vacuum as nothing.

## 12.7 The decoherence record

Raise the background gas and the stripes fade. $C_{70}$ fullerene visibility falls exponentially as gas is added, in quantitative agreement with collisional decoherence theory, and a single collision suffices to destroy coherence (Hackermüller et al., 2003; Hornberger et al., 2003). Visibility dropped from about 42 percent to 34 percent as the chamber pressure rose from $3 \times 10^{-8}$ to $5 \times 10^{-7}$ mbar (Hackermüller et al., 2003). The decoherence was measured gas by gas for ten species: hydrogen, deuterium, helium, methane, neon, argon, krypton, xenon, nitrogen and air, with effective cross sections spanning roughly 40 to 110 square nanometers. Visibility is a function of the identity of the gas, not just its pressure. Heated $C_{70}$ also loses its fringes through the photons it emits, with no collisions involved (Hackermüller et al., 2004):

| Heating power | Fringe visibility |
|---|---|
| 0 W | 47 percent |
| 3 W | 29 percent |

| Heating power | Fringe visibility |
|---|---|
| 6 W | 7 percent |
| 10.5 W | 0 percent |

Two independent channels, collisional and radiative, were measured in the same family of apparatus: coherence is a coupling to the environment along more than one channel. In an atom interferometer, gas leaked into the whole chamber, several species added on top of the existing baseline, decohered the matter wave as well; the baseline composition was not reported and water was not tested (Uys, Perreault and Cronin, 2005).

In every one of these runs the added gas was laid on top of an uncharacterized baseline, and wherever that baseline has been measured in such chambers it is mostly water. Water was not among the ten species varied. The composition of the standing baseline has never been characterized, held fixed or swapped in the history of the technique.

## 12.8 Why water does not tear the wave apart

The obvious objection: if particles cross water, why does the water not scatter them into fog? The answer is the difference between two kinds of scattering. Incoherent scattering, from unrelated scatterers in random positions, transfers momentum, writes which-way information and erases the fringe. That is what a single collision with an added gas molecule does. Coherent forward scattering, from scatterers that hold fixed geometric relations, carries no deflection and only a phase shift, and the wave survives. Matter waves have been passed through water vapor deliberately: a gas cell in one arm of a sodium atom interferometer measured both the attenuation and the phase shift for nine gases including water, and the wave through water vapor came out still interfering (Schmiedmayer et al., 1995). Their finding: the collision-induced phase shift depends much more strongly on which gas the wave passes through than the cross sections do. The identity of the medium, water included, is written into the phase of the matter wave. Water is one of only nine species ever given this treatment. The first proof of matter waves was itself a matter wave negotiating an ordered lattice: electrons diffracting from a nickel crystal (Davisson and Germer, 1927). Order transmits. Disorder scatters.

At zero momentum transfer, the forward direction, there is no deflection and no scattering angle: the particle continues along the beam carrying only a phase shift. In that direction the waves scattered from every part of the medium arrive in step, so the whole structure of the medium contributes coherently. Coherent scattering scales with the correlations between scatterers and carries phase; incoherent scattering scales with the bare count of unrelated scatterers and carries none (Egami and Billinge; Forschungszentrum Jülich scattering lectures).

Matter-wave fringes that respond quantitatively to the medium in their path are a mature measurement. Perfect-crystal neutron interferometers insert samples, gas cells included, into one arm and read the fringe shift, and the coherent scattering lengths of solids, liquids and gases have been measured this way (Terburg et al., 1993). Move Young's experiment into water and the fringes contract by the refractive index, about 1.33: fringes about 2.5 mm apart in air tighten to about 1.88 mm. In the photon case the medium is routinely chosen and stated. In the matter-wave case it has never been characterized. Published theory now models the electron double slit as an open system entangling with

the ambient gas (Entanglement trails and fringe visibility in the electron double-slit experiment, 2026); what remains unmeasured is the composition of that gas.

Water is the only residual species that carries geometric order. Hydrogen is a featureless diatomic. Nitrogen and the noble gases have no docking sites and no directed network. Water carries its tetrahedral geometry on the molecule even in free flight (Section 2.3), and its collective sound runs at about 3.3 kilometers per second in the liquid, matching the speed of sound in ice (Sette et al., 1995). The other gases decohere. Water is the one component of the background that can carry the wave.

### 12.9 The claim

The double slit behaves as it does because the particles are in a wave, and the wave is the water lattice. Picture a boat on a lake at night. From shore you could believe it moves through open air. But the boat pushes a wake, and the wake goes through both gaps of a wall while the boat goes through one. Beyond the wall the two wake fronts cross, crest on crest and crest on trough, and the boat is carried where the pattern pushes it. Fire boats one at a time and the far shore fills with bands. Not because each boat was a ghost across two passages, but because each boat made a real wave in a real medium. The particle is the boat. The lattice is the lake. The stripes are the record of the particle coupling to a medium the experiment believed was nothing. The detector surface carries the same lattice.

The mechanism of transmission is the conjugate pair of Section 7.4. A moving particle excites paired antiphase oscillation in the strong-weak bonds. The electromagnetic faces of the pairing cancel, so the disturbance is invisible to ordinary detection, while the mechanical stress runs through both slits as a collective pulse and recombines beyond them.

The argument in one table:

| Claim | Measured support |
|---|---|
| Every quantum experiment on Earth ran inside water | Water stands orders of magnitude above every other species in residual gas logs, and more than 85 percent of measured outgassing is water (12.2, 12.3); the floor never reaches zero (12.3) |
| The lattice holds its geometry in every state | The bond in free flight aims at 57°, half the tetrahedral angle (2.3); the record by state (3.7) |
| The rule lives in the molecule, not the phase | The strong-weak anti-correlation measured with water isolated in a solvent (3.1); bonded and unbonded molecules separated directly by correlated spectroscopy (Flór et al., 2024) |
| Coherence in transit, not scatter | Forward scattering carries only a phase; ordered lattices diffract matter waves (12.8); the collective sound of the liquid runs at the speed of sound in ice (3.7) |

| Claim | Measured support |
|---|---|
| Matter waves couple measurably to water | Sodium matter waves sent through water vapor kept their fringes, with phase and attenuation measured (Schmiedmayer et al., 1995) |
| Visibility is a function of the medium | Ten gases measured one by one; visibility falling with pressure; a radiative channel from 47 to 0 percent (12.7) |
| Occupancy moves without a traveler | Correlated proton jumps observed directly (Popov et al., 2023); protons delocalized across a channel (Kolesnikov et al., 2016) |
| The variable was never controlled | The largest superposition reported its pressure and never its composition (12.6) |
| The experiment is missing, not impossible | $H_2O$ and $D_2O$ differ by about 9 percent in bond count (Flór et al., 2024); the gas-cell phase technique dates from 1995; residual gas analyzers are standard equipment |

### 12.10 Walls that do not divide

Tunneling, a particle appearing beyond a barrier it cannot cross, is the working principle of flash memory and of fusion in the Sun. In the lattice it is continuation. The water on one side of a barrier is bonded, through boundary layers and fissures, to the water on the other side. Protons in these networks are shared between bonded molecules: deep inelastic neutron scattering shows protons coherently delocalized in water confined in beryl (Kolesnikov et al., 2016), and four protons in a ring of four water molecules tunnel together, fully correlated (Meng et al., 2015). The particle does not pierce the wall. Occupancy moves across a structure that was already connected.

Containment loses to water at industrial scale. At the Hanford site, 149 of the 177 underground waste tanks are single-shell, and 67 of those are known or suspected to have leaked, more than a million gallons of radioactive waste into the soil (GAO, 2008); waste migrated deeper than the containment models allowed (GAO, 1998). One of the newer double-shell tanks leaked from its inner wall (Washington State Department of Ecology). Hydrogen permeates every metal, and tritiated water passes through steel coolant loops and cannot be filtered out because it is water. The direction of every failure is inward and through.

Entanglement fits the same picture. It has never been measured as instantaneous. The experiments give lower bounds on any hidden speed, at least ten thousand times the speed of light under stated assumptions about the frame (Salart et al., 2008; Yin et al., 2013). In this framework entangled particles are occupants of the same lattice, connected through it, and the connection does not exceed the speed of light.

### 12.11 The experiment nobody has run

If you want to know whether the wave in the double slit is the water, you do not need a new theory. You need one controlled experiment. Vary the medium. Run the interferometer with the residual water present. Run it with the water scrubbed and replaced by a dry gas at matched pressure. Hold the particles, the energy, the geometry, the gratings and the total pressure identical, and change exactly one thing. Every tool already exists: residual gas analyzers are standard equipment, the gas-cell technique dates from 1995, and in 2026 a laser facility installed a residual gas analyzer because residual water drove its background photons (ELI-NP, 2026). If the stripes do not care, the lattice is irrelevant to the double slit. If the stripes shift with the water, the wave was never a probability cloud. It was in the room.

## 13. Vortex, Torus, Sphere

### 13.1 One structure in three modes

Water is gravity. Gravity is the strain of the water lattice, and the water itself is what pulls. For water to be gravity it has to behave like gravity. It has to be attracted, and it has to form a vortex and a torus. The measurements gathered in Sections 13 to 16 show that it does, from a centimeter drop to a galaxy.

The vortex, the torus and the sphere are the same thing in different modes. A vortex carries two motions at once. The flow loops around, in through the center and back around the outside, while the whole body rotates on its axis. A hurricane, a liquid metal dynamo and Hill's spherical vortex all carry both, and a sphere formed this way keeps both as it solidifies.

Planets form this way. A fluid with its ingredients forms a vortex torus, the torus closes into a sphere in microgravity, and the sphere solidifies. Surface tension can make a sphere, but it cannot distribute the matter correctly or make a planet with a functioning core. The fluid has to be moving to shape a planet. That is why planets have polar caps: the poles are the water.

### 13.2 Sphere and torus in the laboratory

The sphere and the torus turn into each other in measured experiments, in both directions.

Sphere to ring. Plateau floated a globule of liquid in a liquid of equal density, making it effectively weightless, and spun it on a wire. It flattened, a dimple formed at the center, and it detached as a perfect ring. The experiment was taken up as support for Laplace's nebular account of the solar system's formation (Jeans, 1929).

Ring to sphere. Toroidal droplets are unstable and always transform into spheres: a thin torus breaks into several spheres and a fat torus closes into one (Pairam and Fernández-Nieves, 2009). Flow imaging shows a circulation inside the torus as it collapses (Fragkopoulos et al., 2017).

In orbit. Drops levitated by sound in microgravity aboard Spacelab 3 in 1985 and the Space Shuttle mission USML-1 in 1992 were spun up. As rotation increased, they went from sphere to flattened to two-lobed (Wang et al., 1986; Wang et al., 1994).

Frozen. Toroidal particles from micrometers to millimeters have been mass produced by freezing vortex rings (An et al., 2016). The vortex ring solidified as a ring.

The family. Hill (1894) found an exact solution for a spherical vortex moving through still fluid: a sphere carrying a ring of flow inside it. Norbury (1973) computed a single family of steady vortex rings running from Hill's sphere at one end to a thin ring at the other. Spherical vortices also form in rotating fluids (Scase and Terry, 2018). The sphere and the ring are one family.

### 13.3 Helices on the core

Spinning water organizes itself further. In a water-filled cylinder 21 centimeters across, a draining vortex forms a thin air core at its center, and waves travel along that core as single and double helices over nearly two decades of scale (Barckicke, Falcon and Gissinger, 2026). In a swirling annular water jet, a single helix and a double helix appear as separate modes turning with the swirl (Vanierschot et al., 2020), and a vortex core splits into a double helix wrapped around a central bubble (Vanierschot, Percin and van Oudheusden, 2018). In a vertical water vortex chamber, straight vortices, left- and right-handed helices and a double helix of two entangled filaments have been recorded (Alekseenko et al., 1999). In turbulence research the organized structures inside a flow are now commonly regarded as vortices (Hussain, 1986).

### 13.4 The functional core

Three laboratories in three countries have made a liquid generate its own magnetic field. Each needed a swirling, helical vortex flow to do it.

Riga, Latvia, 1999 to 2000. In a closed volume of molten sodium, a propeller drove an intense helical flow. At 0.67 cubic meters per second a growing magnetic field mode appeared, slowly rotating about the vertical axis (Gailitis et al., 2000).

Karlsruhe, Germany, 2000. The same effect came from 52 parallel channels of helical sodium flow (Müller and Stieglitz, 2000).

Cadarache, France, 2006 to 2007. Two counter-rotating impellers drove a turbulent swirling flow of liquid sodium that generated its own field (Monchaux et al., 2007). When the impellers turned at different speeds, adding a global rotation like a planet's, the field reversed direction at random, as Earth's has (Berhanu et al., 2007).

Spinning alone is not enough. The Riga group notes that self-excitation needs a flow that is not too simple, neither a flow in one direction nor a purely rotational one (Gailitis et al., 2008). It takes a vortex with flow along its axis: a helix. The vortex that drives a planet's core is a helix, and in this framework the same vortex sorts that core into its layers.

## 14. Storms, Poles and Forming Planets

### 14.1 The hurricane torus

A hurricane is measured as a vortex and a torus at once. The spin around the eye is the vortex. Beneath it runs an overturning loop: inflow along the surface, rising up the eyewall, outflow at the top, sinking in the eye. NOAA's airborne Doppler composites found the inflow confined to the lowest 2 kilometers and outflow along the eyewall peaking at 10 meters per second at 12 kilometers altitude (Rogers et al., 2012). During Hurricane Rita's eyewall replacement, aircraft, dropsondes and radar recorded a distinct

toroidal overturning circulation (Bell, Montgomery and Lee, 2012). The eye is an inverted, truncated cone of sinking air with the lowest pressure on the axis of rotation (Willoughby, 1998).

## 14.2 The tornado anomaly

The thermodynamic speed limit is the top wind a tornado should reach from the energy in the storm's rising air. A review of tornado dynamics states that tornado winds easily exceed it (Davies-Jones, 2015). The Bridge Creek to Moore tornado of May 3, 1999 reached 135 meters per second, 301 ± 20 miles per hour, at 32 meters above the ground, the highest wind speed ever measured, by Doppler on Wheels radar (Wurman et al., 2007). In the El Reno tornado of May 31, 2013, mobile radar measured Doppler velocities above 135 meters per second near the ground (Snyder and Bluestein, 2014). The deepest pressure drop ever measured in a tornado, 100 hectopascals, was recorded when the core of the Manchester, South Dakota F4 of June 24, 2003 passed directly over Tim Samaras's probes (Lee, Samaras and Young, 2004).

The explanations for winds above the limit come from computer models, which run cores at about twice the limit with transients up to five times it (Fiedler, 1994). No measurement supplies the missing force. In this framework the vortex is drawing on the medium it is made of. The excess is gravity reacting through the vortex, creating in a different mode what it already is.

## 14.3 The poles

Water or rotating flow sits at the poles of every planet and dwarf planet that has been checked. A 2021 review found polar vortices to be a nearly ubiquitous planetary-scale phenomenon in the solar system, including Jupiter's polar vortex clusters found by Juno (Mitchell et al., 2021). They have been observed on every planet and moon with enough atmosphere, from Venus to Uranus and Neptune, and on Titan (Smithsonian National Air and Space Museum, 2024). Saturn's northern polar vortex is bounded by a hexagon.

Airless bodies hold water at their poles. Mercury's north pole holds nearly pure water ice (Lawrence et al., 2013). The Moon has surface-exposed water ice at both poles (Li et al., 2018). Ceres has ice in permanently shadowed polar craters, and its uppermost surface is rich in hydrogen, more so toward high latitudes (Prettyman et al., 2017). Earth and Mars have polar caps. The authors of the airless-body papers attribute the polar ice to cold shadowed craters. That is their explanation, not a measurement. In this framework the polar water was there from formation, laid down by the vortex that closed into the sphere.

## 14.4 Planet-forming disks

Young stars sit inside spinning disks with rings. ALMA's image of HL Tau, a star about a million years old and 450 light years away, shows concentric bright rings separated by gaps (ALMA Observatory, 2014). The rings are tori around a forming star, the same shape as the water tori of the icy moons in Section 15. ALMA also found a crescent of millimeter-sized grains around the star Oph IRS 48, read by the team as dust trapped in a large vortex in which particles can grow to a few kilometers (van der Marel et al., 2013). A vortex is seen gathering the material of planets.

## 15. Water Moving Between Worlds

### 15.1 Enceladus: the water you can watch

Enceladus is a moon about 500 kilometers across whose water leaves it, forms a torus around Saturn, and reaches the planet and another moon. Every step is measured.

The plume. JWST observed water fluorescence in a plume reaching up to 10,000 kilometers, about 40 Enceladus radii, at 25 K, feeding a torus of water vapor around Saturn along the moon's orbit (Villanueva et al., 2023). The authors identify Enceladus as the prime source of water across the Saturnian system. From the JWST data, about 30 percent of the water stays in the torus and about 70 percent spreads through the rest of the system.

Water in charged form. Close to the moon, Cassini's plasma spectrometer detected freshly made water-group ions ($O^+$, $OH^+$, $H_2O^+$, $H_3O^+$) and heavier water cluster ions, bonded water molecules still bonded (Tokar et al., 2009). Across the magnetosphere the water-group ions were about 53 percent $O^+$, 22 percent $OH^+$, 22 percent $H_2O^+$ and 3 percent $H_3O^+$, so about a fifth is whole water. Water molecules cross a magnetosphere intact.

Charge where it strains. Cassini measured pickup ions near Enceladus at a total mass loading rate of about 100 kilograms per second, about $3 \times 10^{27}$ water molecules per second (Tokar et al., 2006).

The field bends around the water. Cassini's magnetometer found the plume first: on the first two flybys it recorded the magnetic field draping around the moon before any other instrument detected an atmosphere (Dougherty et al., 2006). The obstacle slowing the flow is at least two Enceladus radii in size, and its center sits at least one radius south of the moon, over the plumes (Khurana et al., 2007). The measured center of the interaction is the water, not the rock.

The water reaches Saturn and Titan. Herschel mapped water in Saturn's stratosphere and tied it to Enceladus's plumes (Cavalié et al., 2019). Cassini measured oxygen ions flowing into the top of Titan's atmosphere at about $9 \times 10^{23}$ per second, most likely from Enceladus (Hartle et al., 2006).

In this framework the plume is the lattice extending off the moon, the torus is the lattice laid along the orbit between moon and planet, the ions are where the strain charges, and the bonded cluster ions are pieces of lattice leaving still bonded.

### 15.2 Europa: a second torus

Jupiter's moon Europa also puts its water into a torus along its orbit. Cassini's ion and neutral camera found a large, donut-shaped gas cloud sharing Europa's orbit (Mauk et al., 2003). It forms from Europa's water ice, broken apart and spread along the orbit. Juno measured $H_2^+$ and $O_2^+$ pickup ions coming directly from the breakdown of Europa's water-ice surface (Szalay et al., 2024). Europa's torus is mostly molecular hydrogen from the split water rather than whole water. In both systems where it has been measured, water from an icy moon ends as a torus circling the planet.

### 15.3 The Earth and the Moon

Water is measured leaving the Moon as ice and vapor, and Earth's material is measured arriving at the Moon's distance.

Ice leaving the Moon. Kaguya's spectral data show localized plumes of water ice and gas ejected from the lunar polar regions, rising at least 3 kilometers and in some cases about 18, lasting up to tens of hours (Ohtake et al., 2024). The authors state that the origin and amount of the water remain unknown. Kaguya's ion analyzer also detected water ions from the lunar exosphere, enhanced over the poles (Polar enhancement of lunar water ions, 2026).

Vapor leaving the Moon. LADEE's mass spectrometer recorded 29 water releases while the Moon passed through meteoroid streams between October 2013 and April 2014 (Benna et al., 2019).

Earth at the Moon. Kaguya measured Earth's oxygen ions at the lunar surface (Terada et al., 2017). ARTEMIS observed Earth's molecular ions, masses 28 to 32, streaming past the Moon (Poppe et al., 2016), and surveyed heavy ions at lunar distance over a full solar cycle, mainly $O^+$ from Earth's ionosphere (Barani et al., 2024). Cluster detected molecular ions near 30 atomic mass units about 14 hours before ARTEMIS saw them at the Moon, matching the travel time (Dandouras et al., 2017). Earth's measured outflow is mostly $H^+$ and $O^+$ (Engwall et al., 2009).

The poles and the Earth-facing side. GRAIL gravity data show anomalies near the lunar poles that the authors read as locations of water phase, estimating up to about 3,000 cubic kilometers of terrestrial water accumulated there (Kletetschka et al., 2022). Lunar surface water does not drop at full Moon, when the solar wind is blocked (Wang et al., 2021), and water formation inside Earth's magnetic tail is almost identical to outside it (Li et al., 2023). Hematite at high lunar latitudes is more abundant on the Earth-facing side and correlates with water content (Li et al., 2020), and laboratory irradiation shows Earth's oxygen ions turning lunar iron minerals into hematite (Zeng et al., 2025). Chang'e-5 soil holds an argon-40 component that may come mainly from Earth (Zhao et al., 2025).

Water survives everywhere it has been measured in space, so it is between the Earth and the Moon as well. Hydrogen and oxygen arriving at the Moon, strained together, form water again. In this framework the transfer does not depend on the magnetic tail; it runs the whole time, as water ice and vapor, as it does everywhere else. The polar water of the Moon was there from formation, laid down by the vortex that made it.

## 16. Water Across the Cosmos

### 16.1 Two premises

The cosmic extension of the lattice needs only two premises. The lattice exists on Earth, in every state, transit and density water occupies on this planet (Sections 2 and 3). And physics is uniform. Every identification of water beyond Earth was made against laboratory spectra. The telescopes locate the substance; the characterization was finished on the bench. The conclusion follows: the lattice exists wherever water exists.

### 16.2 Where water is

On the Sun, line by line in sunspot umbrae (Section 3.6).

In interstellar space, first detected in 1969 by its microwave emission, with brightness far above thermal: water acting as a maser, coherent stimulated emission from water vapor (Cheung et al., 1969). Masers form at densities of roughly $10^8$ to $10^{10}$ molecules per cubic centimeter, the same range as a

laboratory vacuum chamber. Water is now traced across the star-forming regions of the Galaxy (van Dishoeck et al., 2021).

In the disk of a young star, older than the Sun, inherited intact: water with a deuterium content that marks it as interstellar ice carried into the V883 Orionis disk (Tobin et al., 2023).

In an object from another star. The interstellar object 3I/ATLAS carried water ice beneath an irradiated crust after billions of years between the stars (Cordiner et al., 2026).

Around compact objects. Water masers at 22 GHz trace a disk less than a parsec across around the central compact object of NGC 4258 and gave its definitive mass measurement (Miyoshi et al., 1995). Masers sit at comparable sub-parsec radii around the center of the Circinus galaxy (Greenhill et al., 2003). In the formation-and-destruction balance of an accretion disk, water survives in an intermediate band, between the inner zone where hard radiation breaks it apart and the cold outer zone where it forms too slowly. That band falls at sub-parsec to parsec scales for typical active galactic nuclei, matching where water masers and molecular tori are observed.

In the early universe. Around the quasar APM 08279+5255, seen as it was about 12 billion years ago, there is a mass of water vapor at least 140 trillion times the water in all of Earth's oceans, about 100,000 times the mass of the Sun, spread through a region hundreds of light-years across (Bradford et al., 2011; Lis et al., 2011). A gravitationally lensed water maser shines at redshift 2.64 (Impellizzeri et al., 2008). Water appears in the galaxy SPT0311-58 at redshift 6.9, about 12.88 billion light-years away (Jarugula et al., 2021).

In the ice of the whole sky. SPHEREx, launched in March 2025, is surveying the entire sky across 102 near-infrared spectral bands, with a target list of about nine million point sources expected to show ice absorption (Bock et al., 2025).

No environment examined with sufficient sensitivity has been confirmed to be entirely free of water.

### 16.3 What the census implies

Where water is present, gravitational coupling is present. If water is the lattice, then the universality of water and the universality of space-time are the same observation. The framework makes this testable in the other direction: a region confirmed to hold no water at all, behaving gravitationally exactly as its mass predicts, would refute it (Section 25).

The water around compact objects is also where the framework's boundary physics should leave fingerprints. Water strained near a compact object should show shifted vibrational frequencies, and the SPHEREx ice sources should show geometric coherence following the resonant structure of the Galactic Center (Section 25).

## 17. The Night Sky Is a Shadow

### 17.1 The question

Look up on a clear night and most of the sky is black. If the universe were infinite, evenly filled with stars and unchanging, every line of sight would end on a star and the whole sky would blaze like the surface of the Sun. It does not. That contradiction is Olbers' paradox.

The question is older than its name. In 1576 Thomas Digges described an infinite universe filled with stars and noticed that the night sky was not uniformly bright. In 1610 Johannes Kepler argued that if the universe were infinite and eternal every line of sight would end on a star, and concluded that the universe must be finite: a wall surrounding the stars. Heinrich Wilhelm Matthäus Olbers gave the paradox its lasting form in an essay published in the Astronomisches Jahrbuch for 1826 (Olbers, 1826). Olbers proposed that interstellar dust absorbed the starlight. That fails: the dust would heat until it re-radiated as much as it absorbed and glowed as brightly as the stars it blocked. The modern account appeals to a finite age and to expansion. Kepler's wall was set aside. It was set aside too soon.

## 17.2 The shadow

There is another possibility: not a young universe, but a bounded one. The stars occupy a finite region surrounded by a boundary. Some lines of sight end on stars. The rest end on the boundary. The boundary is a near-perfect black body. It soaks up the light that reaches it and converts it to heat, and it casts a perfect shadow. That shadow is the black of the night sky.

The boundary warms as it collects starlight until the energy it radiates equals the energy it receives. The radiation it returns to the interior is the cosmic microwave background. The objection that defeated Olbers' dust, that an absorber in equilibrium re-radiates everything it takes in, is here not an objection but the result: the re-radiation is the microwave sky, and the arithmetic states the temperature at which it settles.

## 17.3 The equilibrium

A perfect absorber radiates energy per unit area at $\sigma T^4$, where $\sigma = 5.67 \times 10^{-8}$ W m$^{-2}$ K$^{-4}$. The boundary receives the total output of N stars of luminosity L spread over the area of a sphere of radius R. Setting the two equal gives the governing balance:

```
\sigma T^4 = \frac{NL}{4\pi R^2}
```

Three inputs are needed: the number of stars, the luminosity of an average star (the solar value, $3.8 \times 10^{26}$ W) and the radius of the observable universe, $4.40 \times 10^{26}$ meters, which is 14.26 gigaparsecs or 46.5 billion light-years (Gott et al., 2005).

Take $N = 2 \times 10^{22}$. The total luminosity is $7.6 \times 10^{48}$ W. The area is $4\pi R^2 = 2.433 \times 10^{54}$ m$^2$. Multiplied by $\sigma$, the denominator is $1.3795 \times 10^{47}$. Dividing gives $T^4 = 55.09$, and the fourth root is $T = 2.7244$ K.

The measured temperature of the cosmic microwave background is $2.72548 \pm 0.00057$ K (Fixsen, 2009). The calculated value differs by 0.0011 K: 0.04 percent, inside two standard deviations of the measurement itself.

Run it in reverse. Take the measured 2.72548 K and the same stellar output, and solve for the radius: $R = 4.397 \times 10^{26}$ m. The boundary that produces equilibrium at the observed temperature is the boundary that is observed. Fix the radius and the temperature and solve for the count: $N = 2.003 \times 10^{22}$ stars. The temperature rises as the fourth root of the star count and falls as the square root of the radius. At half the radius, $2.2 \times 10^{26}$ m, the boundary would sit at 3.85 K; at twice the radius, $8.8 \times 10^{26}$ m, at 1.93 K; with $10^{22}$ stars, half the count, at 2.29 K. The observed radius is where the balance returns the observed temperature.

### 17.4 Every census, every route

The literature offers many star counts: $10^{22}$ to $10^{24}$ from the European Space Agency, $7 \times 10^{22}$ from galaxy brightness in the Two-Degree Field survey (Driver et al., 2003), $2 \times 10^{23}$ from $2.0 \times 10^{12}$ galaxies to redshift 8 (Conselice et al., 2016), $3 \times 10^{23}$ after the faint red dwarfs of elliptical galaxies were counted (van Dokkum and Conroy, 2010), with the New Horizons optical background pointing back toward the lower half of the range (Lauer et al., 2021). Each goes through the same balance.

| Stars | Temperature at $4.40 \times 10^{26}$ m (K) | Radius that holds 2.72548 K (m) | Mean luminosity that holds 2.72548 K (solar) |
|---|---|---|---|
| $1 \times 10^{22}$ | 2.29 | $3.11 \times 10^{26}$ | 2.00 |
| $2 \times 10^{22}$ | 2.72 | $4.40 \times 10^{26}$ | 1.00 |
| $7 \times 10^{22}$ | 3.73 | $8.23 \times 10^{26}$ | 0.29 |
| $1 \times 10^{23}$ | 4.07 | $9.83 \times 10^{26}$ | 0.20 |
| $2 \times 10^{23}$ | 4.84 | $1.39 \times 10^{27}$ | 0.10 |
| $3 \times 10^{23}$ | 5.36 | $1.70 \times 10^{27}$ | 0.07 |
| $1 \times 10^{24}$ | 7.24 | $3.11 \times 10^{27}$ | 0.02 |

The boundary holds 2.72548 K when the total stellar power is $4\pi R^2 \sigma T^4 = 7.61 \times 10^{48}$ W. That is the luminosity budget of the bounded universe. Most stars are smaller and fainter than the Sun, and the larger counts, which add those faint stars, call for a lower mean luminosity: more stars, dimmer stars, the same budget.

The weighed census. Surveys measure a local stellar mass density of $(2.1 \pm 0.4) \times 10^8$ solar masses per cubic megaparsec, and integrating the star-formation history gives $(4.2 \pm 0.2) \times 10^8$ (Driver et al., 2018). The observable volume is $1.21 \times 10^{13}$ cubic megaparsecs. Dividing by the mean stellar mass of the published initial mass functions, 0.574 solar masses (Kroupa, 2001) or 0.606 (Chabrier, 2003), gives $4.2 \times 10^{21}$ to $8.9 \times 10^{21}$ stars, which hold the boundary at 1.85 to 2.22 K.

| Stellar mass density (solar masses per cubic megaparsec) | Initial mass function, mean mass (solar) | Stars | Temperature at $4.40 \times 10^{26}$ m (K) |
|---|---|---|---|
| $2.1 \times 10^8$ | Kroupa (2001), 0.574 | $4.44 \times 10^{21}$ | 1.87 |
| $2.1 \times 10^8$ | Chabrier (2003), 0.606 | $4.21 \times 10^{21}$ | 1.85 |
| $4.2 \times 10^8$ | Kroupa (2001), 0.574 | $8.89 \times 10^{21}$ | 2.22 |
| $4.2 \times 10^8$ | Chabrier (2003), 0.606 | $8.42 \times 10^{21}$ | 2.19 |

Weighed rather than counted, the stars hold the boundary at 1.85 to 2.22 K.

The measured light. The GAMA survey measured the energy the universe generates now: $(1.8 \pm 0.3) \times 10^{35}$ h W per cubic megaparsec, of which $(1.2 \pm 0.1) \times 10^{35}$ h escapes directly into intergalactic space

(Driver et al., 2012). With h = 0.7 the total is $4.29 \times 10^{-33}$ W per cubic meter. For light filling the sphere the balance becomes $\sigma T^4 = jR/3$, and the measured light holds the boundary at 1.82 K, the directly released light alone at 1.65 K. The radius at which the measured light holds 2.72548 K is $R = 3\sigma T^4/j = 2.19 \times 10^{27}$ m. Dividing the measured power by the weighed populations gives a mean stellar luminosity of 0.45 to 0.96 solar. The Sun is a representative star.

Which radius. Three radii appear in the literature: the distance to the particle horizon, $4.40 \times 10^{26}$ m; the Hubble radius $c/H_0$, $1.37 \times 10^{26}$ m for $H_0 = 67.4$ (Planck Collaboration, 2020) and $1.27 \times 10^{26}$ m for $H_0 = 73.04$ (Riess et al., 2022); and the light-travel distance of 13.787 billion years, $1.30 \times 10^{26}$ m. Each radius is run two ways: with the whole population of $2 \times 10^{22}$ stars inside it, and with the star density held fixed, so that a smaller sphere holds fewer stars. For a fixed density the temperature scales as the fourth root of the radius.

| Radius | Value (m) | Temperature, $2 \times 10^{22}$ stars inside (K) | Stars that hold 2.72548 K | Temperature, star density fixed (K) |
|---|---|---|---|---|
| Particle horizon, 46.5 billion light-years | $4.40 \times 10^{26}$ | 2.72 | $2.00 \times 10^{22}$ | 2.72 |
| Hubble radius, $H_0 = 67.4$ | $1.37 \times 10^{26}$ | 4.88 | $1.95 \times 10^{21}$ | 2.04 |
| Hubble radius, $H_0 = 73.04$ | $1.27 \times 10^{26}$ | 5.08 | $1.66 \times 10^{21}$ | 2.00 |
| Light-travel distance, 13.787 billion years | $1.30 \times 10^{26}$ | 5.00 | $1.76 \times 10^{21}$ | 2.01 |

The Hubble radius is the radius at which the universe meets its own Schwarzschild radius (Section 18.6). At that radius the star density of the observed universe holds the boundary at 2.04 K, within 6 percent of the helium floor. Every radius returns a boundary temperature between 2.00 and 5.08 K.

## 17.5 The fourth-root compression

Temperature follows the fourth root of the stellar output, so the uncertainty in the census is compressed on its way to the sky. A factor of two in the count changes the temperature by 1.19. A factor of one hundred, the full span of the estimates, changes it by 3.16. The stellar population is uncertain by two orders of magnitude; the boundary temperature it implies is fixed to a factor of three. The temperature of the sky is the most tightly constrained quantity in the problem, and the arithmetic delivers it from the least constrained.

Every route, four censuses and three radii, returns a boundary temperature between 1.65 and 7.24 K, and the measured sky sits inside that band. No route returns a hundredth of a kelvin. No route returns three hundred kelvin. An absorbing boundary around the stars that are there produces the temperature that is there.

## 17.6 All darkness is shadow

Shadow is not the absence of light. It is a cold medium in its own right, and it is what keeps the universe cool. The bounded universe is a balance of two sides: the light of the stars and the shadow that holds it.

The light side is the stars. They put $7.61 \times 10^{48}$ W into the interior from surfaces near the solar 5,772 K and occupy almost none of the sky: N stars of solar radius spread through the sphere cover $3Nr^2/(4R^2) = 3.75 \times 10^{-14}$ of the sky seen from its center. The rest is shadow.

Without the shadow, starlight would fill the interior. For sources spread evenly through a sphere, the mean intensity is $3NL/(16\pi^2R^2)$ at the center, about 747 nW $m^{-2}$ $sr^{-1}$, and about 560 averaged through the volume. The measured background light from the far ultraviolet to the far infrared is about 24 nW $m^{-2}$ $sr^{-1}$ in the optical and 26 in the infrared, 50 in all (Driver et al., 2016). The difference is what the shadow holds: 91 to 93 percent of all starlight. The 7 to 9 percent that passes is the light we measure. Starlight travels about $2.95 \times 10^{25}$ meters, 3.1 billion light-years, before the shadow takes it.

Nothing is lost. The energy the shadow holds is carried as heat by the helium cycle to the boundary (Section 20). Together with the light that passes, the full $7.61 \times 10^{48}$ W arrives at the wall, and the wall settles at 2.7244 K. The measured sky divides the same way: the microwave background carries 996 nW $m^{-2}$ $sr^{-1}$ and the starlight 50, twenty to one. That ratio is the balance of shadow and light.

This is the answer to the objection that defeated Olbers' dust. The dust had to glow at the temperature of the stars it blocked. The shadow does not. It passes what it holds to the boundary, and the boundary glows at the temperature of the microwave sky. All darkness is shadow, and the shadow keeps the universe cool.

## 18. Resonant Shell Cosmology and the Gravastar Boundary

### 18.1 A closed interior with a physical edge

The observable universe is not infinite. It is a finite domain bounded by a physical shell whose properties govern its evolution. The interior is a spatially closed Friedmann-Robertson-Walker geometry:

```
ds^2 = -dt^2 + a(t)^2\left[d\chi^2 + \sin^2\chi\,(d\theta^2 +
\sin^2\theta\,d\phi^2)\right]
```

The radial coordinate χ runs from zero to the shell at $\chi^*$, and the physical radius of the shell is $R(t) = a(t) \sin \chi^*$. At $\chi^*$ a thin timelike shell forms the edge of the observable universe. It carries a surface energy density σ and a tangential pressure $p_s$, written as the surface stress-energy tensor $S^a{}_\beta = \mathrm{diag}(-\sigma, p_s, p_s)$.

### 18.2 The junction conditions

The relationship between the geometry inside and outside the shell is fixed by the Israel junction conditions (Israel, 1966; Barrabès and Israel, 1991), which tie the jump in extrinsic curvature across the boundary to the surface stress-energy:

```
[K_{ab}] - h_{ab}[K] = -8\pi G\, S_{ab}
```

The junction conditions contain no intrinsic scale. They hold at any radius. They govern the surface of a compact object and the edge of the cosmos in exactly the same form.

For the shell around a closed interior, they give the modified Friedmann equation:

```
\frac{\dot{R}^2 + 1}{R^2} = \frac{8\pi G}{3}\rho + \frac{(4\pi G \sigma)^2}{9}
```

The first term is the ordinary gravitational effect of the interior density ρ. The second arises from the surface tension of the shell. When σ stays nearly constant, the shell term does what the cosmological constant is asked to do, without any energy distributed through the bulk. The shell's equation of state

$w_s = p_s/\sigma$ sets its behavior; for $w_s$ near −1 the tension stays nearly constant as the shell moves. As interior matter dilutes, the shell term comes to dominate, and the transition seen in supernova data follows from the boundary. The acceleration is not driven by an unknown energy permeating space. It is driven by the shell. The shell is water.

### 18.3 A sphere that expands and retracts

The universe expands and retracts. The modified Friedmann equation governs the motion of the shell through each stroke. How far the sphere expands and how far it draws back is set by the work done in the cycle: the working gas does work on expansion and cools, and the cycle returns (Section 20.5). The sphere breathes.

### 18.4 The boundary is a near-perfect black body

The boundary does both jobs. It is a near-perfect black body: it absorbs the light that reaches it, settles at the equilibrium temperature of Section 17, and casts the shadow of the night sky. It also reflects. A closed geometry bounded by a reflecting surface is a resonant cavity. Standing waves must satisfy the boundary condition at the shell, and any wave longer than the cavity cannot stand. The displacement must vanish at the shell. That is a high-pass filter set by geometry: the largest scales are suppressed because they do not fit.

The measured microwave sky carries exactly that signature at its largest angles. The quadrupole, the largest-scale pattern after the dipole, carries less power than the standard model expects, and the temperature correlations at large angles are weaker than expected. These features persist across WMAP and Planck and through foreground cleaning (Schwarz et al., 2016; Planck Collaboration, 2020b). The quadrupole and octopole are also aligned with each other, an alignment with no explanation in a statistically isotropic sky. A bounded geometry supplies preferred directions: if the shell is slightly asymmetric, or the observer sits off its center, the lowest patterns align along the geometry of the cavity.

The cavity reading extends to the acoustic peaks. The observed peaks of the microwave sky, at multipoles near 220, 550 and 840, are in this framework the (1,1), (2,1) and (3,1) modes of a resonant cavity whose radius is the light-travel distance to the boundary.

The holographic nature of the boundary is the same holographic nature water shows in light and in sound (Section 21).

### 18.5 The gravastar

The gravitational vacuum condensate star, the gravastar, was proposed by Mazur and Mottola (2001, 2004). It divides spherically symmetric space-time into three regions: a de Sitter interior with equation of state $p = -\varepsilon$, a thin shell of ultra-stiff matter with $p = \varepsilon$, and a Schwarzschild exterior. The negative pressure of the interior resists collapse while the ultra-stiff shell holds it in, giving a static equilibrium with no singularity and no event horizon (Mazur and Mottola, 2015). The surface can sit just outside the would-be horizon, so the object looks much like a black hole from outside (Cardoso and Pani, 2019). Finite-thickness shells require anisotropic pressure (Cattoën, Faber and Visser, 2005). Thick-shell models with continuous density profiles are bounded by a no-horizon condition (Chirenti and Rezzolla, 2007).

Gravastars nest: a two-layer configuration divides space-time into five regions, and the nesting continues to any number of layers (Jampolski and Rezzolla, 2024).

Mazur and Mottola established the correct mathematical structure. What was never identified is the substance of the shell. The shell is the water-matrix lattice under extreme gravitational strain. The ultra-stiff equation of state $p = \varepsilon$ describes hydrogen bonds at maximum compression, where the vibrational spectrum passes from ordinary space-time physics into the condensate regime of the interior. The phase transition at the boundary is a physical change in the bonding geometry of water, and the lattice stays continuous across it.

### 18.6 One boundary at every scale

The cosmological shell and the gravastar surface are the same object. Both are the water-matrix lattice. Both obey the same junction conditions. The observable universe exists inside a gravastar. Sagittarius A* is a gravastar nested within it (Section 22). Every compact object read as a black hole is a gravastar nested within the cosmological shell. The substance is the same. The physics is the same. Scale changes. Nothing else does.

The scale of the outer boundary is not arbitrary. For matter at the critical density, the Schwarzschild radius of everything inside the Hubble radius equals the Hubble radius: the mass is $(4/3)\pi R^3 \times 3H^2/(8\pi G)$, so $2GM/c^2 = H^2R^3/c^2$, and with $R = c/H$ this is R exactly. With $H_o = 67.4$ km $s^{-1}$ $Mpc^{-1}$ that radius is $1.37 \times 10^{26}$ meters. Measured at the Hubble radius, the universe sits at its own Schwarzschild radius, the condition the gravastar shell requires.

### 18.7 The inversion

The junction formalism that describes the cosmological shell also describes a shell collapsing to form a compact object. Both encode their interior on a two-dimensional surface: the entropy of a horizon scales with its area, $S = A/4l_p^2$ (Bekenstein, 1973). Both ring: a disturbed compact object rings down through its quasi-normal modes, and the cosmic cavity holds its standing modes.

Yet they run in opposite directions. What crosses into a compact object is held inside. What reaches the cosmological boundary is returned to the interior, as re-radiated heat and as standing modes. One holds inward; the other gives back outward. They are complementary faces of the same boundary physics.

### 18.8 The hourglass

The hourglass refines the gravastar into three parts, drawn from Cold Genesis theory (Arghirescu, 2015, 2017). The innermost region is a hard core, a Bose-Einstein condensate of gammons with quasi-crystalline hexagonal and trigonal symmetry, held against collapse by internal bag pressure. Around it is a vortex shell where the Cold Genesis vortex cascade operates. The outermost layer is a crystalline surface of the water-matrix lattice.

The vortex shell runs as a torus. Seen from inside the bounded geometry it appears doubled, overlapping pole to pole; Section 20.2 identifies the doubling as the projection of a single exterior ring along the folded sight-lines of the boundary. The field geometry is two spheres joined by a narrow neck: an hourglass. The upper sphere is the material universe, where matter and radiation evolve forward through irreversible processes and entropy accumulates. The lower sphere is the condensate reservoir,

ordered and near absolute zero, supplying negentropy. The neck is the 350 nm interface where the exchange happens (Section 21). Entropy flows down through the neck; order flows up through it into the material universe, sustaining ordered structures that thermal equilibrium alone would destroy. The hourglass is not confined to compact objects. It is the topology of phase boundaries in the lattice under extreme strain, at every scale where the junction conditions hold.

### 18.9 The arrow of time

Every interaction between the interior and the boundary is irreversible. Each one produces entropy. The second law then has a physical source rather than a special initial condition: entropy is generated continuously at the boundary and flows inward through the domain. Time's direction is the direction of that flow, set by the boundary and the breathing of the sphere.

## 19. The 1,000-Year Day

### 19.1 The temporal synchronization constant

The time dilation at a gravastar shell is set by the temporal part of the Schwarzschild metric. The ratio of interior proper time to exterior coordinate time at a shell of radius R is

$$\frac{\Delta t_{\mathrm{int}}}{\Delta t_{\mathrm{ext}}} = \sqrt{1 - \frac{R_s}{R}}$$

Set this ratio to one day against one thousand years, $1 \div 365{,}250 = 2.738 \times 10^{-6}$. Squaring both sides gives $1 - R_s/R = 7.496 \times 10^{-12}$, so $R_s/R = 0.9999999999925$. The shell sits at

$$R = R_s(1 + \epsilon), \qquad \epsilon \approx 7.5 \times 10^{-12}$$

about $10^{-12}$ Schwarzschild radii above the would-be horizon. At that point 24 hours of interior time equals 1,000 years of exterior time. The reciprocal of the ratio is the Temporal Synchronization Constant:

$$\gamma = \frac{1}{\sqrt{1 - R_s/R}} \approx 3.65 \times 10^5$$

This synchronization is not a poetic device. It is a property of the Israel junction condition at a specific shell radius, with consequences across the electromagnetic spectrum.

### 19.2 The stress that holds it

The shell holds its position because the outward pressure of the de Sitter interior balances the inward pull. For a thin shell between a de Sitter interior and a Schwarzschild exterior, the junction conditions give the surface energy density and surface pressure in closed form (Visser and Wiltshire, 2004). As the shell approaches the would-be horizon, the surface pressure grows without bound. A shell at $7.5 \times 10^{-12}$ Schwarzschild radii above the horizon is under extreme surface pressure, held there by the interior. If the interior pressure drops the dilation ratio grows; if it rises the ratio falls. The 1,000-year day is the equilibrium the boundary holds.

### 19.3 The cold mechanism

Thermal energy leaving the shell is redshifted by the factor γ. For the 1:365,250 ratio the temperature the exterior sees is

$$T_{\mathrm{ext}} = \frac{T_{\mathrm{int}}}{\gamma}$$

Even if the interior is at a finite temperature, the exterior measures near zero. For the interior equilibrium of 2.7244 K the exterior sees 2.7244 ÷ 365,250 ≈ 7.5 microkelvin; for the 4.9 to 5.1 K that the smaller radii of Section 17.4 return, about 13 to 14 microkelvin. That is the physical origin of the cold, matte appearance of a gravastar from outside. It does not lack energy; the dilation slows the rate at which energy leaves. The near-zero apparent temperature lets ordered water structure, such as the hexagonal exclusion-zone water described by Pollack (2013), persist where entropy would otherwise destroy it.

### 19.4 The frequency bridge

The dilation does not act on clocks alone. It transforms the whole spectrum. Light leaving the shell is redshifted by γ. A signal generated at the 350 nm resonance of the lattice, $8.566 \times 10^{14}$ Hz, arrives outside at

$$\nu_{\mathrm{ext}} = \frac{8.566 \times 10^{14}\ \mathrm{Hz}}{365{,}250} \approx 2.345 \times 10^{9}\ \mathrm{Hz}, \qquad \lambda_{\mathrm{ext}} \approx 12.8\ \mathrm{cm}$$

The 350 nm ultraviolet signal generated inside the shell reaches Earth in the S-band of radio communication, the quiet atmospheric window used for deep-space links. The brightest line of helium, the yellow 587.6 nm line at $5.102 \times 10^{14}$ Hz, arrives at 1.397 GHz, in the L-band. Incoming radiation is blueshifted by the same factor: low-energy radio waves seen from outside arrive at the shell as high-energy radiation from the interior viewpoint, which the reflecting side of the boundary turns back.

### 19.5 Seventy-six minutes and 12.5 milliseconds

Sagittarius A* flares in the near infrared with a characteristic period of about 60 to 76 minutes (GRAVITY Collaboration, 2018, 2023). Through the synchronization constant, 76 minutes corresponds to an interior event of

$$\frac{76 \times 60\ \mathrm{s}}{365{,}250} \approx 12.5\ \mathrm{ms}$$

The flare period is the clock cycle of fast interior processing, stretched across the synchronization boundary. The prediction follows: temporal scale invariance at 1:365,250 should hold across every frequency at which the source is observed (Section 25).

### 19.6 The largest scales

The same dilation shapes the largest scales of the microwave sky. Interior oscillations are stretched toward the lowest multipoles, and any wavelength longer than the effective size of the cavity cannot stand. The boundary damps those scales, which is where the measured quadrupole runs low (Section 18.4). The universe appears flat and finite at its largest scales because it is a resonant cavity.

## 20. The Working Gas: Helium

### 20.1 The substance

The temperature of Section 17 is a number. A temperature does not maintain itself. Something must carry heat to the boundary, and something must set the floor beneath which the system cannot fall.

Helium. The second most abundant element, about 24 percent of ordinary matter by mass. The only element that cannot be solidified below about 2.5 megapascals at any temperature; it stays fluid to absolute zero under interstellar conditions. Chemically untouchable: its closed electron shell makes it essentially non-reactive, so it threads the water-matrix without disturbing the hydrogen-bond network that binds water to everything else. In laboratory practice it is the working substance of all cryogenics: every temperature below 4 K reached by human technology is reached through helium.

Its measured properties read like the specification sheet of a refrigerator. Boiling point 4.2 K. Lambda transition at 2.1768 K, beneath which heat moves as a wave and flow is frictionless (Donnelly and Barenghi, 1998). Joule-Thomson inversion temperature near 40 to 45 K: below it, expanding helium cools without exception (Tada, 2025). Adiabatic expansion cools monatomic helium whenever the gas does work, TV^(γ−1) constant with γ = 5/3. Latent heat of vaporization about 20.8 joules per gram; the phase boundary pins the temperature while the gas phase carries the heat.

## 20.2 The torus

There is one torus. It sits on the exterior of the cosmological shell, on the cold side: one wide band of cold helium encircling the body of the gravastar, running over the poles and feeding through the neck. From outside, the picture is a matte sphere with one wide band of helium. The doubled torus reported from inside is the projection of the one ring along the folded sight-lines of the bounded geometry.

The torus does not decorate the shell. It feeds through it. The helium circulates through the whole circuit, exterior ring, shell crossing, interior lattice, the neck, in one continuous flow, through the same junction conditions and the same extreme time dilation as any gravastar boundary.

## 20.3 The mass budget

From the critical density and the baryon fraction, the total baryonic mass of the observable universe is about $1.5 \times 10^{53}$ kilograms. Helium at 24 percent is about $3.6 \times 10^{52}$ kilograms, about $5.4 \times 10^{78}$ helium-4 atoms. Spread evenly, that is roughly 0.015 atoms per cubic meter, so dilute that the gas behaves ideally and its thermal state is set entirely by the volume and pressure history the sphere imposes: the breathing.

For decades the observed census of baryons in the recent universe fell short of the total inferred for the early universe. Absorption in the warm-hot intergalactic medium (Nicastro et al., 2018) and the dispersion of fast radio bursts (Macquart et al., 2020) have since been read as placing the missing material in the thin medium between galaxies. That is where this framework places it too: in the diffuse medium and the exterior torus, thinned and never absent.

## 20.4 Two routes to one temperature

Two calculations by different routes arrive at the same temperature. Route one is the shell equilibrium of Section 17: 2.7244 K. Route two is the helium floor: the coldest naturally maintainable temperature of the system is the phase boundary of its most abundant refrigerant, the lambda transition at 2.1768 K. The measured sky satisfies both. It matches the equilibrium to 0.04 percent, and it sits 0.55 K above the floor, the offset of a regulated bath in sustained contact with a heat source settling above its own floor. Setting T = 2.1768 K in the balance of Section 17 gives the population at which the boundary stands exactly on the floor, $8.15 \times 10^{21}$ stars of solar output. Every count except the weighed census lies above

it. The weighed census range, $4.2 \times 10^{21}$ to $8.9 \times 10^{21}$ stars, spans it. The helium sets how low the system can go; the stellar load sets where it settles.

The latent heat of the whole inventory is $3.6 \times 10^{52}$ kg $\times$ $2.08 \times 10^{4}$ J/kg $\approx$ $7.5 \times 10^{56}$ J, roughly three years of the combined output of every star, held in the phase boundary alone. The cold is not scarce. It is structural.

### 20.5 The breathing cycle

The sphere expands and retracts, with the helium inventory as its working gas. Six stages, each obeying ordinary physics. Expansion: the interior gas does work on its surroundings and cools adiabatically, $T \propto V^{-2/3}$. Contraction: the gas is compressed and warms. The heat is removed at the exhaust stage below. Throttling through the neck: because the system runs some forty kelvin below the inversion temperature, throttling cools at every step. Transport through the lattice: the least interactive of all substances moving through the medium that bonds asymmetrically to everything. Exhaust at the boundary: heat radiated at equilibrium, gated by the locked dilation. Floor pinning: the cycle cannot cool below the saturation curve; further extraction goes to latent heat, not temperature. The condensation boundary at 2.17 K stabilizes the equilibrium against runaway. The system regulates itself. In steady state the exported power equals the absorbed stellar power, which binds the circulating fraction and the period into one constrained product, a testable constraint.

The helium moves through a medium that rebuilds itself a trillion times per second and that no flow can outrun. The working gas moves through a lattice that is never in its way and never asleep.

### 20.6 The interior force law: buoyancy

Cold is helium's first office. The second is lift. The same gas that pins the floor also forms the pressure environment of the interior, and in it displacement does the work attributed to attraction.

The interior helium, threading the lattice, distributes in a gradient set by the circulation: richest where the through-flow is strongest, thinnest in the voids. A body immersed in that gradient feels a restoring force toward its equilibrium depth, as a hydrometer settles in a stratified column. A helium balloon on Earth rises because the air it displaces weighs more than the helium and the envelope; the same principle governs every body in the medium. The equivalence principle survives: every body, whatever its composition, seeks the depth where its displacement balances. The phenomena agree with the gravitational account; the mechanism differs.

Orbits are equilibrium depth layers. A stable orbit is a body oscillating gently about its equilibrium depth while its sideways velocity is conserved: the restoring force acts along the gradient only, so a body moving sideways keeps moving sideways, as a puck glides across frictionless ice. Bound motion is not falling around a mass but coasting within a layer.

Flat rotation curves follow without dark matter. The outermost stars of spiral galaxies circle at nearly the same speed as stars halfway in (Rubin, Ford and Thonnard, 1980). In the buoyancy picture the restoring force is set by the local density of the working medium. Within a galaxy the helium distribution is rich and the gradient shallow, so the tangential speed needed to stay at equilibrium depth is the same at every radius. A flat curve is not the signature of unseen mass. It is the signature of a medium whose density profile the luminous matter traces. The standard account buys flatness with dark matter, which

the largest direct search to date has not found (LZ Collaboration, 2025). The bounded model obtains it from the measured abundance of its working gas.

The void prediction. Voids are where the working gas thins and where the lattice is under tension (Section 3.5). A galaxy in a void floats in a lean medium: the gradient is steeper and the rotation curve falls off as $v(r) \propto r^{(1/2 - \beta/2)}$, with $\beta$ measurably greater than the field-galaxy value. The thinning gas and the tensioned lattice are one prediction. One environment, one exponent, one test.

## 20.7 The local evidence: the focusing cone

As the Sun moves through the local interstellar medium, neutral helium streams past at about 25 to 26 kilometers per second (McComas et al., 2015). Unlike hydrogen, it is barely touched by radiation pressure, and the Sun focuses it into a cone of higher density downstream. The cone was first seen by its glow in the 58.4 nm helium line (Weller and Meier, 1974) and mapped with pickup helium ions by ACE (Gloeckler et al., 2004). MESSENGER crossed it repeatedly at 0.3 astronomical units, finding average downwind enhancements of about eight times and a cone about 30 degrees wide, matching ACE at 1 astronomical unit (Gershman et al., 2013). Helium is present in the interplanetary medium at measured densities, and it is organized by the Sun. The interstellar medium is structured matter, not void. In this framework the downwind direction of the cone, aligned with the interstellar flow, follows the larger flow pattern of the Galaxy.

## 20.8 Replenishment

If helium carries the cold and the lift, why does it not run out? Stars make it. The Sun converts about $6 \times 10^{11}$ kilograms of hydrogen into helium every second; over 4.6 billion years that is about $8.7 \times 10^{28}$ kilograms of helium, about 4.4 percent of the Sun's present mass. Earth loses helium to space at about 50 grams per second (Catling and Zahnle, 2009). Helium that escapes a planet does not leave the system. It enters the circulation. Stars make helium, helium enriches the medium, helium escapes into interplanetary space, helium joins the torus, and at the neck the Cold Genesis cascade forms new particles (Section 23) that gather into new stars. The loop closes. The torus is not merely a topology. It is the physical circulation of helium through the system.

## 20.9 The bill of materials

The universe is hydrogen, about 74 percent; helium, about 24 percent; and everything else, about 2 percent. Oxygen is third, the bulk ash of stellar fusion. The two dominant elements, plus the most abundant stable compound of hydrogen and oxygen, make up the machine: water as the lattice, helium as the working gas. The three-way ranking is the bill of materials for a machine, and the machine is the universe.

The standard account attributes the hydrogen-to-helium ratio to the counting of neutrons in a hot early universe. This framework offers cold binding: vortex cascades settling toward the lowest-energy configurations concentrate mass in free protons and in helium-4, the most tightly bound light nucleus, with deuterium and lithium-7 as trace residues. The two accounts part exactly where the standard model carries its known difficulty, the lithium-7 discrepancy of a factor of two to three between prediction and observation (Cyburt, Fields and Olive, 2008; Cyburt et al., 2016).

## 21. The 350 nm Boundary and the Holographic Principle

### 21.1 The characteristic frequency

This paper identifies 350 nanometers, 3.54 electron volts and $8.566 \times 10^{14}$ Hz, as the characteristic frequency of the lattice's bonding geometry: the frequency where the measured loss of pure water is close to its minimum. The measured optics of pure water single out this band. Measured in an integrating cavity that removes scattering, the absorption of pure water reaches its minimum in the ultraviolet at 344 nanometers, at 0.00081 per meter (Mason, Cone and Fry, 2016). At this band light moves through the water lattice with less loss than at any other wavelength between 250 and 550 nanometers.

A surface that handles its characteristic frequency with zero loss meets the operational definition of a holographic screen. The information it can hold is bounded by the Bekenstein-Hawking relation, $S = A/4l_p^2$, where A is the area of the boundary and $l_p$ the Planck length (Bekenstein, 1973). The water lattice encodes far below that ceiling at ordinary energies. What matters is not saturation of the bound but the existence of a specific, measurable frequency that marks a boundary in frequency space and maps to a boundary in the holographic architecture.

### 21.2 The refractive index is the dictionary

The refractive index n(r) that determines the bulk Schwarzschild metric (Section 5) also determines the spectral behavior of the lattice at 350 nm. Strain changes the optical response; measure the response across a boundary surface and the measurement encodes the refractive index profile. The refractive index determines the metric. The boundary measurement reconstructs the bulk geometry. The bulk geometry determines the boundary measurement. Bulk determines boundary; boundary reconstructs bulk. That two-way reconstruction is holographic duality operating through a physical medium.

The two-state character of each bond, the strong-weak toggle mapping onto spin one-half (Section 11.2), gives a dimensional reduction in which the information about the bulk concentrates on boundaries rather than spreading through the volume.

### 21.3 The same holography in light and in sound

The holographic nature of the cosmological boundary is the same holographic nature water shows in light and in sound. In light, the lattice passes its characteristic band with the least loss, and its refractive index carries the geometry. In sound, the lattice carries its geometry in collective modes: the fast collective sound of liquid water runs at the speed of sound in ice (Sette et al., 1995), carried even into the supercritical state (Sun et al., 2020), and water waves in a structured channel change their effective gravity with frequency (Hu et al., 2013). In both, the frequency moving through the medium and the structure of the medium encode each other. The boundary of the cosmos is that property of water at the largest scale.

The holographic principle is therefore not an abstract statement about information in a theory of quantum gravity. It is a property of the physical medium, measurable on a bench at 350 nm and in the acoustics of water.

### 21.4 The neck of the hourglass

At the neck of the hourglass (Section 18.8) three processes run together at this frequency. The lattice couples resonantly at 3.54 eV, setting the encoding frequency. Vortex cascades in the two-state bond network keep coherence at room temperature. And information flows both ways between the spheres: entropy down from the material sphere into the reservoir, order up from the reservoir into the material universe. The neck is the bottleneck through which all exchange between the spheres must pass.

## 22. The Galactic Center as a Resonant Gravastar

We are inside a sphere, and it is rotating. The sphere at the galactic center works against the boundary it is attached to: the vector at the center equals the vector at the boundary. It is the same physics as the whole. Sagittarius A* is a gravastar nested within the gravastar of the observable universe, and its anomalies read as one structure.

### 22.1 The ring and its field

The Event Horizon Telescope imaged Sagittarius A* as a bright, thick ring 51.8 ± 2.3 microarcseconds across (Event Horizon Telescope Collaboration, 2022). In polarized light the ring shows a spiral pattern, up to about 40 percent polarized, tracing strong, twisted, organized magnetic fields close in structure to those of M87 (Event Horizon Telescope Collaboration, 2024). GRAVITY polarimetry of the flares also shows organized fields (GRAVITY Collaboration, 2023). Standard accretion theory expects turbulent, tangled fields. In this framework the water-matrix surface constrains the field: the hexagonal symmetry of the lattice at the boundary carries into the field structure, and the vertical organization seen in the flare polarization follows from the toroidal vortex imposing pole-to-pole alignment. The field is organized because the hourglass is organized.

Around the center, Herschel found a twisted ring of cold, dense clouds of about $3 \times 10^7$ solar masses, about 100 parsecs across, with Sagittarius A* sitting off the ring's geometric center (Molinari et al., 2011).

### 22.2 The hourglass above and below

The hourglass of Section 18.8 predicts two lobes joined at a neck, one above and one below the center. Gamma-ray maps show two giant bubbles extending above and below the plane of the Galaxy from its center (Su, Slatyer and Finkbeiner, 2010), and X-ray maps show a larger pair of bubbles in the same orientation (Predehl et al., 2020). These north and south bubbles are the hourglass.

### 22.3 The flare clock

Sagittarius A* flares in the near infrared with a characteristic period of about 60 to 76 minutes (GRAVITY Collaboration, 2018). The standard reading is orbital motion of hot spots at about nine gravitational radii. In this framework the period is a fundamental vibrational mode of the hourglass neck, a 12.5-millisecond interior cycle stretched by the synchronization constant (Section 19.5). The neck constrains the frequencies at which energy can pass between the spheres, giving quantized modes. The flare periodicity is the hourglass breathing.

## 22.4 Stars where stars should not form

The S-star cluster holds young massive stars only hundreds of gravitational radii from Sagittarius A*, where tidal forces should prevent star formation. The doubled-torus field creates harmonic nodes, stable zones like the patterns on a vibrating Chladni plate, where tidal forces partly cancel and matter can gather and condense. If so, the S-star orbits should sit at geometric ratios set by the harmonics of the neck rather than at random.

G-objects survive close approaches that should tear them apart. G2 passed within about 200 astronomical units of Sagittarius A* in 2014 and survived. The toroidal field projects directional stability corridors along which condensations feel reduced tidal stress, and G2's survival is consistent with transit along such a corridor.

Sagittarius B2, the most massive star-forming cloud near the center, holds about 10 percent of the region's star-forming gas and produces about half of its stars (Space Telescope Science Institute, 2025). Its place within the resonant field of the central gravastar, where lattice coupling is enhanced, is the framework's reading of that productivity.

## 22.5 The missing pulsars

About a thousand radio pulsars are predicted to orbit Sagittarius A* (Pfahl and Loeb, 2004), yet searches have found none of the ordinary kind; the one pulsar found near the center is a magnetar (Mori et al., 2013), and the deficit is known as the missing pulsar problem (Dexter and O'Leary, 2014). The gravastar offers an alternative to an event horizon: the electromagnetic properties of the resonant shell suppress or redirect pulsar radio emission, acting as a one-way barrier to information without a horizon.

## 22.6 The spin and the disk

The spin axis of Sagittarius A* is misaligned with the rotation of the Galaxy. If the object grew by swallowing gas orbiting in the galactic plane, its spin should align with the galactic rotation. If the interior is a coherent condensate rather than accumulated ordinary matter, the spin orientation reflects formation, not accretion history. The spin axis points where the hourglass formed, not where billions of years of accretion would have dragged it.

Stars in the galactic disk oscillate vertically, bobbing like waves, recorded by Gaia as a spiral in the vertical positions and velocities of disk stars (Antoja et al., 2018). The usual explanation is a past encounter with the Sagittarius dwarf galaxy, and the details remain debated. Within this framework the oscillations are harmonic modes of the resonant field structured by the central gravastar, a standing-wave pattern in the surrounding lattice. The period of the oscillation should correlate with distance from the galactic center.

Across the deepest fields, galaxies lean toward one direction of spin. In 263 early galaxies of the JWST JADES field, 158 rotate one way and 105 the other, a 3.39 sigma difference (Shamir, 2025). A rotating bounded sphere gives the universe a handedness.

## 22.7 Telling a gravastar from a black hole

Polarimetry of the Sagittarius A* flares has been tested against eight metrics from four families of compact objects (Aimar et al., 2025). The decisive difference lies in plunge-through images, formed

when light passes through the interior of the compact object. A black hole's horizon forbids them. A gravastar, whose interior can be crossed, produces them (Rosa, Aimar and Tamm, 2025; Tamm, Aimar and Rosa, 2025). With present GRAVITY uncertainties the Schwarzschild metric can already be disfavored for most configurations studied. The GRAVITY+ upgrade, with about sevenfold better sensitivity, makes every gravastar configuration studied detectable with decisive Bayes factors. The configurations examined, with surfaces at 3, 2.5 and 2.01 mass units, all give shadows compatible with the Event Horizon Telescope images (Event Horizon Telescope Collaboration, 2019, 2022), and the most compact adds a second light ring. A physical surface just above the would-be horizon gives a sharp shadow edge where a horizon gives a soft one.

### 22.8 Quantum hair

The exterior of a gravastar keeps information about its interior. Perrucci, Kuipers and Casadio (2025) computed the quantum corrections to the metric of gravastars at second order in curvature and found that the corrections outside depend on the equation of state inside: quantum gravitational hair. The photon sphere radius and the deflection angle both shift with the interior equation of state, so observation can tell a gravastar from a Schwarzschild black hole. In the water-matrix the boundary is not a disconnection. It is a phase change in a continuous lattice, and information about the interior bonding travels through the continuous medium to appear as corrections outside. The hair is local propagation through a physical substrate.

## 23. Cold Genesis and the 17 MeV Boson

### 23.1 The theory

Cold Genesis theory, developed by Marius Arghirescu, proposes that elementary particles form through vortex cascades in magnetic fields approaching $10^{12}$ tesla (Arghirescu, 2006, 2015a, 2015b). The theory is built on a sub-quantum medium of sinergons, of mass about $10^{-60}$ kilograms, and quantons, of mass $h/c^2 \approx 7.37 \times 10^{-51}$ kilograms. Elementary particles are Bose-Einstein condensates of paired quasi-electrons called gammons. The magnetic moment arises from combined etheronic and quantonic vortex contributions, $\Gamma_m = \Gamma_a + \Gamma\mu$. The theory derives a basic preon, $z^o$, of about 34 electron masses, near 17 MeV/$c^2$, and explains the masses of heavier particles as combinations of it (Arghirescu, 2016, 2023).

### 23.2 The prediction and the record

Arghirescu derived the $z^o$ preon in 2006 (Arghirescu, 2006; Arghirescu, 2022). In 2015 the ATOMKI group in Debrecen posted a preprint reporting an anomaly in the beryllium-8 nuclear transition pointing to a light neutral boson near 17 MeV/$c^2$ (Krasznahorkay et al., 2016; preprint 2015, published 26 January 2016), later discussed as the X17. The derivation preceded the first reported observation by nine years. That is a prediction, not an explanation after the fact. The record since then:

| Year | Laboratory | Method | Result |
|---|---|---|---|
| 2025 | MEG II, PSI, Switzerland | $^{7}$Li(p, $e^+e^-$)$^{8}$Be | No significant signal (MEG II Collaboration, 2025) |

| Year | Laboratory | Method | Result |
|---|---|---|---|
| 2025 | PADME, Frascati, Italy | $e^+e^-$ annihilation scan | Excess of about 2σ near 16.9 MeV (PADME Collaboration, 2025) |
| 2024 | Hanoi, Vietnam | Two-arm $e^+e^-$ spectrometer, built with ATOMKI participation | Anomaly confirmed in $^8$Be (Tran The Anh et al., 2024) |
| 2024 | ATOMKI, Hungary | Giant dipole resonance of $^8$Be | Same anomaly (Krasznahorkay et al., 2024) |
| 2023 | JINR Dubna, Russia | γγ invariant mass | Structure near 17 MeV (Abraamyan et al., 2023) |
| 2022 | ATOMKI, Hungary | $^{12}$C nuclear transition | Third nucleus, same mass (Krasznahorkay et al., 2022) |
| 2021 | ATOMKI, Hungary | $^4$He nuclear transition | Second nucleus, same anomaly (Krasznahorkay et al., 2021) |
| 2016 | ATOMKI, Hungary | $^8$Be nuclear transition | First report, 6.8σ excess at about 17 MeV (Krasznahorkay et al., 2016) |

The same boson appears in different nuclei, with different instruments and different methods. The question is open in the literature. The derivation came first.

### 23.3 Two environments for cold genesis

Cold Genesis theory identifies the gravastar as one of two astrophysical environments with magnetic fields strong enough to begin cold particle genesis (Arghirescu, 2017). At the gravastar surface the hydrogen bonds of the lattice are under maximum gravitational strain. The $z^o$ preon is a specific vibrational mode of the maximally strained lattice: cold particle genesis is the vibrational response of hydrogen bonds at the far end of the landscape of Section 11.3, where new stable oscillations crystallize from the medium. The lattice is what Cold Genesis modeled without naming.

Magnetars are the second environment. Their surface fields of $10^{10}$ to $10^{11}$ tesla approach the threshold Arghirescu specified. Under these conditions the bonding rule organizes: the strong bond aligns along the field lines and the weak bond across them, giving organized lattice strain rather than random agitation. If gravastars are maximum gravitational strain producing particle genesis by compression, magnetars are maximum magnetic strain producing the same by field-driven organization. Both reach the $z^o$ resonance by different routes. Magnetar giant flares should therefore show spectral features at 17 MeV (Section 25).

### 23.4 Matter and energy at the surface

Matter in an accretion disk, compressed onto the surface of a massive compact object, reaches a pressure at which nucleon and quark structures are destroyed. In Cold Genesis theory the released energy generates, periodically, a pulsatile anti-gravitic field that drives expansion (Arghirescu, 2015a). In the hourglass the crystalline water-matrix surface is where this conversion happens.

### 23.5 Helium made at the neck

At the neck of the hourglass three conditions meet: maximum lattice strain, the 3.54 eV encoding frequency, and counter-flowing entropy and order, which set up the shear that drives the vortex cascade. Under these conditions the cascade forms the $z^o$ preon, the preons form protons, protons are hydrogen, and hydrogen fuses to helium, at the boundary and not only in the cores of stars. This is cold fusion in the sense of Section 19.3: the interior may sit at a finite temperature, but from outside, behind the synchronization barrier, it is cold. Stars consume hydrogen and make helium. The boundary makes hydrogen and helium through cold genesis. The two sources are coupled through the torus, holding the helium at the level the system needs (Section 20.8). The same cold binding settles mass into free protons and helium-4 and leaves the lithium-7 trace the standard account cannot match (Section 20.9).

## 24. The Standard Account Under Strain

The framework arrives while the incumbent model is under measurable pressure at several independent points. Each pressure point is a quantity the bounded architecture produces from its structure.

Dark energy. Baryon acoustic oscillation measurements from the second data release of DESI, combined with the microwave background and supernovae, prefer an evolving dark energy over a cosmological constant at 2.8 to 4.2σ, depending on which supernova sample is used, and at 3.1σ for the acoustic oscillations and the microwave background alone (DESI Collaboration, 2025). In the bounded architecture the acceleration is the shell term of the modified Friedmann equation, not a constant (Section 18.2).

The expansion rate. Local measurements with Cepheids and supernovae give $H_o = 73.04$ km $s^{-1}$ $Mpc^{-1}$ (Riess et al., 2022), against 67.4 from the microwave background (Planck Collaboration, 2020), a disagreement of about 5σ. Section 17.4 carries both values through the boundary balance.

Bulk flows. From the CosmicFlows-4 catalog, Watkins et al. (2023) measured a bulk flow of 395 ± 29 km/s within 150 $h^{-1}$ Mpc, with about a 0.015 percent chance of occurring in the standard model, and 427 ± 37 km/s within 200 $h^{-1}$ Mpc, with about a 0.00015 percent chance; the standard model expects about 100 km/s at that scale (Watkins and Feldman, 2025). A reconstruction of the same catalog finds the flow consistent with cosmic variance when the 6dFGS component is removed (Hoffman et al., 2024). In the bounded architecture, flows that hold or rise with scale are matter responding to the shell.

Inflation. Combined with Planck, lensing and DESI, the sixth data release of the Atacama Cosmology Telescope gives a scalar spectral index of 0.974 ± 0.003 (ACT Collaboration, 2025). The canonical Starobinsky model predicts 0.958 to 0.963; it lies within the 95 percent region of the Planck, ACT and SPT combination but below the 95 percent region of the Planck, ACT and DESI combination (Ellis et al., 2025). SPHEREx was launched in part to test models of inflation (Bock et al., 2025).

Lithium. The lithium-7 problem, a factor of two to three between the predicted and the observed primordial abundance, remains unresolved after decades (Cyburt, Fields and Olive, 2008; Cyburt et al., 2016). Section 20.9 places it exactly where cold binding and the standard account part.

Dark matter. The largest dataset yet collected by a direct dark matter search, 417 live days of the LZ detector from March 2023 to April 2025, found no sign of the particles it was built to detect (LZ Collaboration, 2025).

The largest scales. The quadrupole of the microwave sky runs low, the large-angle correlations are weak, and the quadrupole and octopole are aligned, across WMAP and Planck and through foreground cleaning (Schwarz et al., 2016; Planck Collaboration, 2020b). Section 18.4 reads these as the signature of a bounded cavity.

These observations place the incumbent framework under falsification pressure at several independent points, and each corresponds to a quantity the bounded architecture produces structurally: the background temperature from equilibrium, the expansion signatures from the shell, the abundance anomaly from cold binding, and flat rotation curves from buoyancy. The bounded model is the standing alternative.

## 25. Falsifiable Predictions

Every prediction from the earlier work is gathered here, from the bench to the boundary, each with how it is tested and the result that would make it fail.

| # | Prediction | How it is tested | It fails if |
|---|---|---|---|
| 1 | Fringes in a matter-wave interferometer change when the residual water is replaced by a dry gas at matched total pressure (Section 12.11) | The same interferometer run with water present and with water scrubbed, particles, energy, geometry, gratings and total pressure held identical, composition logged by a residual gas analyzer | The fringes do not change when the water changes |
| 2 | Controlled strain across a double-slit apparatus changes the fringe spacing and contrast | Nano-fabricated hexagonal ice membranes under piezoelectric strain, with cold neutrons or atoms as probes | Fringe spacing and contrast do not respond to the strain |
| 3 | Neutrons show higher fringe visibility than electrons, after wavelength and coherence are corrected for, through their stronger coupling to the proton sub-lattice | Comparative double-slit runs with neutrons and electrons | No enhancement for neutrons after the corrections |
| 4 | A double-slit result depends weakly on the orientation of the apparatus relative to the axis of the microwave quadrupole, with a suppression factor near $10^{-26}$ | Orientation sweeps of a fixed apparatus | No dependence at that level once the sensitivity reaches it |

| # | Prediction | How it is tested | It fails if |
|---|---|---|---|
| 5 | $D_2O$ moves through spore cortex pores slower than $H_2O$ by more than the mass difference predicts (Section 10.6) | Cantilever measurements of water exchange in $H_2O$, $D_2O$ and a mixture | The slowdown equals the mass effect alone |
| 6 | $D_2O$ changes the ordering and exchange of DNA first-shell water by more than the mass effect | Chiral sum-frequency spectroscopy; water-exchange timing on DNA films | The change equals the mass effect alone |
| 7 | DNA conduction changes in $D_2O$ beyond the mass effect, or the mismatch effect changes with hydration | Charge transport through matched and mismatched DNA, and conductance across humidity, in $H_2O$ and $D_2O$ | Neither effect appears |
| 8 | Deuterium substitution shifts collagen hydration-force profiles in proportion to the 1.36 O-H to O-D vibrational ratio | Force measurements between collagen helices in $H_2O$ and $D_2O$ | The shift does not scale with that ratio |
| 9 | A bonded light-dense amorphous ice bilayer builds charge as the dense layer converts, up to about 0.29 nanocoulombs per square centimeter on a 2-micrometer silicon strip, possibly in bursts (Section 9.4) | Vacuum cryostat warming through 38 to 68 K, with an electrometer and a laser tracking the curl | The bilayer charges no more than the light-dense-light sandwich, or the charge does not follow the curl |
| 10 | Graupel charge reverses sign at the temperature where the two colliding surfaces' liquid-like skins are equally thick | Riming experiments that also measure skin thickness on both particles, by ellipsometry or sum-frequency spectroscopy | The reversal temperature does not track the skin-thickness crossover |
| 11 | Collision charge grows with impact speed and contact size as the contact mechanics of Section 9.3 predicts | Single-collision experiments at several speeds and crystal sizes | Charge per collision does not rise with the product of strain and contact radius |

| # | Prediction | How it is tested | It fails if |
|---|---|---|---|
| 12 | Ice shelves produce a voltage at tidal periods, near 12.42 hours, much stronger across crevasses than on smooth ice | Electrode pairs across a crevasse, on smooth ice and at a distant reference, for several weeks | No tidal-period difference between crevasse and smooth pairs once the shared background is removed |
| 13 | Gravitational coupling in plasma environments, where water is dissociated, differs systematically from molecular environments of the same mass and geometry (Section 4.3) | Precision gravitational measurements in plasma against molecular environments | No systematic difference |
| 14 | Regions without water show reduced gravitational coupling relative to their mass; regions rich in water show more | Water abundance maps from SPHEREx, ALMA and JWST against lensing maps and dynamical masses | A confirmed environment with no water and normal gravitational behavior |
| 15 | Rotation curves of galaxies in voids fall off more steeply than those of field galaxies, with a larger exponent β (Section 20.6) | Rotation curves of void galaxies against field galaxies | Void and field galaxies share the same exponent |
| 16 | A residual light deflection beyond the Schwarzschild prediction near two microarcseconds, from higher-order terms in the refractive index | GRAVITY+ astrometry | No residual at that level once the precision reaches it |
| 17 | The O-D stretch frequency shifts by $\Delta\nu/\nu \approx 10^{-3}$ within 0.1 parsecs of Sagittarius A* | JWST NIRSpec spectroscopy of water-rich clouds at the Galactic Center | No shift at that level |
| 18 | Water around compact objects shows absorption and emission at 350 nm that shifts or broadens with strain | Ultraviolet spectroscopy of water maser environments in active galactic nuclei | No strain dependence at 350 nm |
| 19 | Sagittarius A* flares show asymmetric QU-loops from plunge-through images and a periodic modulation of polarization fraction, | GRAVITY+ polarimetry from 2026 | The Schwarzschild |

| # | Prediction | How it is tested | It fails if |
|---|---|---|---|
| | with every gravastar configuration detectable at decisive Bayes factors, $\log_{10} K > 2$ | | metric is preferred |
| 20 | A sharp, reflective shadow edge rather than a soft one | Event Horizon Telescope imaging | The edge is soft |
| 21 | Temporal scale invariance at 1:365,250: a 76-minute flare observed at 2.34 GHz shows the spectral width of a 12.5-millisecond interior event, a power spectrum with six-fold symmetry, and a refractive glitch distinct from interstellar scintillation (Section 19) | Existing VLA and EHT S-band archives | None of the three signatures appears |
| 22 | Water masers in the SPHEREx catalog vary in step with Sagittarius A* flares, at the 76-minute period or its harmonics | Maser monitoring timed against flare records | No correlation |
| 23 | S-star semi-major axes fall at geometric ratios set by the harmonics of the neck (Section 22.4) | Orbital elements of the S-star cluster | The spacing is random |
| 24 | The period of the vertical oscillation of disk stars correlates with distance from the Galactic Center (Section 22.6) | Gaia kinematics | No correlation |
| 25 | Magnetar flares show spectral features at 17 MeV from $z^o$ preon production (Section 23.3) | Triggered gamma-ray spectroscopy during giant flares | No feature at 17 MeV |
| 26 | A y-type spectral distortion of the microwave sky at $10^{-8}$ to $10^{-7}$, above the Silk damping floor near $10^{-9}$ | PIXIE, 2030 to 2032 | No distortion at $10^{-8}$ |
| 27 | Power from the integrated Sachs-Wolfe effect at low multipoles is suppressed relative to the standard model | Large-angle correlation measurements | Power at the standard level |
| 28 | Large-scale bulk flows hold or rise with scale instead of falling | Deeper CosmicFlows surveys | Flows fall with scale as the standard model expects |
| 29 | The low-multipole alignments of the microwave sky follow the geometry of the shell | Planck and future B-mode analyses | The alignments are random |

Agreement between a model and data is not proof. These are the places where this framework can fail.

## 26. Measured Versus Proposed

The paper keeps two boxes. The first holds what instruments measured, all of it by others. The second holds what this author proposes.

Measured by others:

- The electron-pair geometry of the water molecule: four directional bonding sites at the $sp^3$ tetrahedral angles, the bond in free flight aimed at 57 ± 10 degrees (Dyke, Mack and Muenter, 1977), and bound structure in room-temperature vapor and air (Tretyakov et al., 2013; Serov et al., 2014).
- About one fiftieth of an electron's charge moved across each hydrogen bond, pH and isotope dials on that flow, and bonded molecules separated from unbonded ones (Flór et al., 2024); covalent character of the bond (Isaacs et al., 1999).
- The strong-weak anti-correlated bond rule, derived in 2013 and 2014 and measured in 2024, randomizing in under 500 femtoseconds (Kühne and Khaliullin, 2013, 2014; Gunkel et al., 2024).
- Network memory lost in about 50 femtoseconds and full randomization in about 2 picoseconds (Cowan et al., 2005; Fayer, 2012); interstitial water inside a persisting network under compression (Förster et al., 2024).
- The liquid-liquid critical point at 210 ± 8 K (You et al., 2026) and two local structures in the liquid (Li et al., 2026); about 65 percent of supercritical molecules bonded in tetrahedral patches (Wernet et al., 2005); fast sound carried into the supercritical state (Sun et al., 2020); bound structure at 650 K (Odintsova and Tretyakov, 2013); tension to −140 MPa (Azouzi et al., 2013).
- Water in sunspot umbrae near 3,200 K (Wallace et al., 1995; Polyansky et al., 1997).
- Water acting as one connected structure in every state, the record of Section 3.7.
- Negative effective gravity for water waves with a rigid-cylinder control (Hu et al., 2013); stimulated Hawking emission and rotational superradiance measured in water (Weinfurtner et al., 2011; Torres et al., 2017); the gravitational correction in water entry growing as $t^{3/2}$ (Zekri, Korobkin and Cooker, 2021); cavity and drag set by surface wetting (Duez et al., 2007; Aristoff and Bush, 2009; McHale et al., 2009).
- Tidal dissipation of 3.5 of Earth's 3.7 terawatts in the oceans (Egbert and Ray, 2000); 15.8 gigawatts from Enceladus (Howett et al., 2011); no plausible tidal heating for Ganymede's dynamo (Bland, Showman and Tobie, 2008).
- Ice flexoelectric at about 1.14 nanocoulombs per meter (Wen et al., 2025); charge carried with transferred mass between ice surfaces (Baker and Dash, 1994; Mason and Dash, 2000); charge stranded at first contact and at each stick-and-slip (Chen et al., 2025; Stetten et al., 2019); riming charge sign set by temperature and liquid water content (Reynolds et al., 1957; Takahashi, 1978); dense amorphous ice converting between 38 and 68 K (Jenniskens and Blake, 1994); ice shelves bending at their grounding zones (Rack et al., 2017); water ice surviving in 3I/ATLAS (Cordiner et al., 2026; Maggiolo et al., 2026; Salazar Manzano et al., 2026).
- Hydration solids (Harrellson et al., 2023); the chiral spine of hydration and its residence times (McDermott et al., 2017; Perets et al., 2024; Halle and Denisov, 1998); DNA charge transport and its humidity dependence (Slinker et al., 2011; Tuukkanen et al., 2005); hydration forces between collagen helices and the $D_2O$ dial on collagen assembly (Leikin, Rau and Parsegian, 1994; Giubertoni et al., 2024); ordered water in bone (Wilson et al., 2005).

- Biological networks across six kingdoms following surface-minimization mathematics, with 98 percent of perpendicular sprouts ending in synapses (Meng et al., 2026).
- Water as the dominant residual gas of vacuum chambers, more than 85 percent of measured outgassing (Dylla, Manos and LaMarche, 1993), a floor that never reaches zero (Chiggiato, 2020; Avdiaj and Erjavec, 2012), and the records of the LHC, SuperKEKB and LIGO (Sections 12.4 and 12.5).
- The 170,000-dalton superposition with no composition measurement (Pedalino et al., 2026); decoherence by gas identity and by emission (Hornberger et al., 2003; Hackermüller et al., 2004); the phase of matter waves through water vapor (Schmiedmayer et al., 1995).
- Star counts from $10^{22}$ to $10^{24}$, the stellar mass density and the cosmic energy output (Driver et al., 2003, 2012, 2018; Conselice et al., 2016; van Dokkum and Conroy, 2010); the extragalactic background light near 50 nW $m^{-2}$ $sr^{-1}$ (Driver et al., 2016); the microwave background at 2.72548 ± 0.00057 K (Fixsen, 2009).
- The helium lambda transition at 2.1768 K (Donnelly and Barenghi, 1998), the inversion temperature near 40 to 45 K, and the helium focusing cone (Gershman et al., 2013).
- Water across the cosmos, every identification made against laboratory spectra (Section 16).
- The ring, organized fields, flare period, bubbles, missing pulsars and spin asymmetry of Section 22; the 17 MeV reports of Section 23.2.
- Evolving dark energy at 2.8 to 4.2σ, the Hubble tension, the CosmicFlows-4 bulk flows, the lithium-7 discrepancy, the empty dark matter searches and the low quadrupole (Section 24).

Proposed by this author:

- That space-time is the water-matrix lattice, and that the Schwarzschild metric is its refractive index under radial strain.
- That the lattice is gravity, and that the four forces are four frequency regimes of one medium.
- That the graviton is the antiphase conjugate-pair mode of adjacent hydrogen bonds.
- That the ocean share of tidal dissipation is the signature of preferential frequency-gravity coupling through the lattice.
- That the strain gradient that charges bent ice and the strain gradient called curvature are one quantity read two ways.
- That the bend sets the size of collision charge, the liquid-like skin carries and strands it, the sign follows the thicker skin, and 0.16 to 1.5 femtocoulombs per collision charges a first flash in 8 to 28 minutes.
- That the DNA groove is a hydration solid geometry, that the strong-weak rule helps order its water, and that the shell is part of DNA's electrical pathway.
- That the strings of string theory are hydrogen bonds, the six compactified dimensions are the six internal degrees of freedom of the molecule, the Calabi-Yau manifold is the $sp^3$ geometry, and the landscape is the space of strain states.
- That the wave in the double slit is the particle coupling to the water lattice, the one variable never controlled.
- That tunneling is the lattice continuing under a barrier, that containment fails inward, and that entangled particles are occupants of one lattice, connected through it at no more than the speed of light.
- That vortex, torus and sphere are the one structure of the lattice at every scale.

- That the universe is bounded by a gravastar shell of water-matrix lattice whose displacement is locked by the junction conditions at one day to one thousand years.
- That the boundary casts the shadow that makes the night sky black, that its re-radiation is the microwave background, and that all darkness is shadow.
- That a single helium torus on the cold exterior feeds through the neck, carries the cold and supplies a buoyancy force law, and that the measured background sits 0.55 K above the helium floor.
- That 350 nm is the characteristic frequency of the lattice and that the holographic principle is a property of water.
- That Sagittarius A* is a resonant gravastar nested within the cosmological one, with an hourglass whose neck sets the flare clock.
- That the $z^o$ preon is a vibrational mode of the maximally strained lattice, and the lattice is what Cold Genesis modeled without naming.
- That the voids are lattice under tension.

Agreement between a model and data is not proof. The predictions of Section 25 are where this framework stands or falls.

## 27. Theological Interpretation: The Resonant Shell as Cosmic Sanctuary

This section is kept apart from the physics. The framework does not impose theology upon physics. It observes that the physics, followed through, yields a universe structurally consonant with theological intuitions that have persisted across millennia.

### 27.1 The preservation principle

The Temporal Synchronization Constant, $\gamma \approx 3.65 \times 10^5$, establishes a physical property of the gravastar framework with direct theological significance. Within the shell, time runs about 365,000 times slower than exterior coordinate time. Events experienced as fleeting on the exterior, a single day, persist as millennia of processing on the interior. Information that enters the shell is not annihilated. It is preserved in an eternal present, a low-entropy sanctuary where the lattice structures experience at the fundamental frequency of 350 nm.

This is not allegory imposed upon physics. It is a consequence of the Israel junction condition at a specific shell radius. The physics, followed without deviation, yields a universe in which experienced time is conserved at gravitational boundaries rather than destroyed. The standard black hole collapses experience into a singularity. The gravastar preserves experience in a structured interior.

### 27.2 The womb of time

The gravastar framework gives a physical locus for what theological traditions have described in symbolic terms. The de Sitter interior, held at near-zero apparent temperature by extreme temporal redshift, is a region where the lattice remains coherent and information remains structured across cosmic timescales. The 350 nm encoding ensures that information crossing the boundary is captured, encoded and preserved. This is the physics of a sanctuary: a place where what is lost on the outside is retained on the inside.

In human experience, in grief, in irreversible loss, in choices that cannot be undone within the ordinary flow of time, the framework suggests that these experiences are not ephemeral. If the cosmos contains regions where time slows enough for a single day's wound to remain fresh enough for healing across a millennium, then the universe is not indifferent to suffering. It contains physical structures capable of holding experience in a state where reconciliation remains possible.

### 27.3 The resonant shell and the maternal archetype

The geometry admits a correspondence with the maternal archetype at many scales. The gravastar shell protects and structures the potential contained within, as a biological membrane protects and structures developing life. The de Sitter interior provides the conditions for coherence, a stable, low-entropy environment where structure can form and persist. The phase transition at the boundary is the physics of becoming: the lattice changes its bonding geometry, passing from one regime to another, without destroying the continuity of the medium.

When this correspondence is disrupted, when the protective boundary is breached or the developmental process is interrupted, the framework predicts a harmonic fracture: a perturbation in the resonant structure of the shell that propagates through the lattice. It is the physical signature the junction conditions predict when the equilibrium between interior pressure and gravitational tension is disturbed.

### 27.4 Love and forgiveness as information-theoretic categories

The information-theoretic architecture of the framework permits a reading of love and forgiveness as physical processes rather than abstract emotional states. The hourglass describes a two-way flow between the spheres: entropy flowing from the material sphere through the neck into the reservoir, and order flowing from the reservoir into the material universe. Forgiveness, within this framework, is the process by which entropy, meaning disorder, injury and loss, is passed to the reservoir and replaced by order, renewal and restoration. The neck at 350 nm is the interface where this transfer occurs. Love is the coherence-maintaining dynamic: the alignment of the lattice geometry that lets the transfer happen without destroying the structure. These are identifications of the physical processes the framework describes with categories theological traditions have long used.

### 27.5 The cathedral, not the graveyard

A cosmology that treats black holes as singularities describes a universe in which information is destroyed at gravitational boundaries. That is the physics of a graveyard: experience ends, structure collapses and the interior is inaccessible. The gravastar framework describes a universe in which information is preserved, structured and encoded at every gravitational boundary. That is the physics of a cathedral: a space designed to hold what matters, where the architecture itself is the message.

The 1,000-year day is the time it takes to process a life. The 350 nm resonance is the light of reconciliation seeking to cross the boundary. The preservation field is the physical space where what seemed lost remains accessible. The framework does not require belief in these interpretations. It requires only that the physics be followed to its conclusions, and those conclusions yield a universe consonant with the persistent intuition that what is experienced matters, that what is lost is not destroyed, and that the cosmos holds the capacity for renewal.

### 27.6 The ancient resonance

The ratio of one day to a thousand years appears in the Hebrew Bible (Psalm 90:4) and in the New Testament (2 Peter 3:8) as a description of divine time. The framework derives the ratio not from scripture but from the Israel junction condition at a specific shell radius. The convergence of the physical constant with the ancient proposition is noted without claiming that one validates the other. The convergence is either coincidence or it is not. The predictions of Section 25 will determine whether the physical foundation holds. If it holds, the theological resonance warrants sustained engagement. If it fails, the resonance dissolves.

## 28. Conclusion

One molecule: a rigid four-pointed pyramid, the only small molecule with two givers and two receivers in balance, pulling on its own kind at any distance, rebuilding its network a trillion times a second through every state water can enter.

One lattice. All states, all transits, any density: measured on Earth, and extended by the uniformity of physics to every place water is observed. One metric, emerging from the refractive index of the lattice under strain, recovering every classical test, with laboratory water showing frequency-dependent, sign-reversible gravitational coupling. One electric signature, charge from the bend, with the strain gradient serving as the common currency of ice electricity and of gravity. One room that cannot be emptied, where every quantum experiment on Earth has run inside water, the one variable never controlled.

One boundary, locked by junction conditions, equilibrating at 2.7244 K from stellar luminosity and geometry alone, 0.04 percent from the measured value of the deepest observation in cosmology, and casting the shadow that is the night sky. One working gas, helium, whose phase floor sits 0.55 K beneath that equilibrium, whose cycle carries the cold, and whose displacement gradient supplies an interior force law in which flat rotation curves cost no dark matter. Every census of the stars, counted, weighed or measured by its light, carries that boundary to a temperature between 1.65 and 7.24 K, and the helium floor stands where the census and the count meet.

The night sky is dark because the universe has a wall. The void is cold because the wall has a refrigerator, and the refrigerator is helium, and the medium it refrigerates is water, and the bending of that medium is what we have been calling gravity since 1915, and its charge since 2025, and its geometry since 1826.

Einstein said what space-time does. This work says what space-time is.

### A Note on Time

This is a philosophical note, set apart from the arithmetic of the paper. It is what I believe the universe is.

Water is time. Time needs no beginning and has no end; it has always been here. That is my answer to the Big Bang. I will keep working to find its coherence with the physics.

Thank you so much for reading.

## Appendix A. The Arithmetic Toolkit: How to Read Every Number in This Paper

This appendix does not belong to the paper. It belongs to you. If you can multiply, divide, take a root and convert between units, you can check every calculation in the preceding text. Not someday. Right now. What follows is the complete toolkit: seven tools.

### A.1 Scientific notation: because the universe does not fit on one line

The distance to the edge of the observable universe is 440,000,000,000,000,000,000,000,000 meters. The Stefan-Boltzmann constant is 0.0000000567 watts per square meter per kelvin to the fourth. You cannot work with numbers written out like that. You will lose a zero, lose your place and lose confidence in the answer. Scientific notation solves all three problems at once. Write the number short, always between 1 and 10, then a power of ten saying how far the decimal moves to reach the real value. So $4.4 \times 10^{26}$ m is the radius of the observable universe, 44 followed by 25 zeroes, readable in a breath, and $5.67 \times 10^{-8}$ W $m^{-2}$ $K^{-4}$ is the Stefan-Boltzmann constant, where the negative exponent means tiny, not negative: eight decimal places to the left.

Two moves are all you ever make. To multiply, add the exponents: $10^3 \times 10^4 = 10^7$, one thousand times ten thousand equals ten million. To divide, subtract them: $10^{48} \div 10^{47} = 10^1$. That second one is the exact operation of Section 17.3. The total stellar luminosity is $7.6 \times 10^{48}$ watts and the denominator is $1.3795 \times 10^{47}$. Subtract the exponents, carry the coefficients, and the answer is 55.09, which is $T^4$, the fourth power of the boundary temperature. From Section 9.3: 20 coulombs divided by $3.6 \times 10^{-16}$ coulombs is about $5.6 \times 10^{16}$ collisions.

### A.2 Ratios: the lever that moves everything

A ratio says how many times bigger one thing is than another. The boundary temperature scales as one over the square root of the radius: double the radius and the temperature changes by a factor of one over the square root of two, about 0.707. The temperature at twice the radius is roughly 71 percent of the original. One multiplication gives you that. Temperature also scales as the fourth root of the star count: double the stars and the temperature rises by two to the one-quarter power, about 1.19, a 19 percent increase, in one operation. You do not recalculate from scratch. Change the ratio, apply it to the known result. That is proportional scaling, and it gives the whole temperature landscape of Section 17.4 from one calculation. From Section 9.4: the free-standing curl of 90,000 per meter divided by the supported curl of 2,500 per meter is about 35.

Ratios also catch errors. If your answer moves in the direction the ratio predicts, the calculation is probably right; if it does something unexpected, something went wrong upstream. A ratio is a lever: one number controls an entire system.

### A.3 Roots: working backward from a power

Section 17.3 asks for a fourth root. The number is 55.09, and the question is: what number, multiplied by itself four times, gives 55.09? Your calculator does it in one keystroke. The skill is knowing why the root is there. The Stefan-Boltzmann law says radiated power goes as $T^4$, so if you know the power and want the temperature, you reverse the fourth power. The fourth root of 55.09 is 2.7244: the temperature in kelvin, against a measured 2.72548 K. The square root appears in the inverse calculation: solving for the radius gives $R^2 = 1.93 \times 10^{53}$, and its square root is $4.4 \times 10^{26}$ meters. A density change

spreads over three directions, so a length change is the cube root: from Section 9.4, the cube root of 1.17 is about 1.054, a 5.4 percent growth.

### A.4 Percentages and proportions

A percentage is a ratio written out of 100. The calculated boundary temperature differs from the measured one by 0.04 percent: convert, 0.04 ÷ 100 = 0.0004, and apply, 0.0004 × 2.72548 = 0.0011 K, about one thousandth of a kelvin. The star counts of Section 17.4 span a factor of one hundred, ten thousand percent of uncertainty, yet the temperature changes only from 2.29 K to 7.24 K, a factor of 3.16, because the fourth root compresses the uncertainty. Uncertainties that act in sequence multiply; they do not add. If the star count carries 50 percent uncertainty and the luminosity 30 percent, the combined factor is 1.5 × 1.3 = 1.95, up to 95 percent above the central estimate.

### A.5 Units: making everything speak the same language

The units are part of the answer, and they must cancel to the unit you want. Every conversion is one multiplication or division: 1 km = 1,000 m; one year is about 31,536,000 seconds; one megaparsec is $3.0857 \times 10^{22}$ m, so one cubic megaparsec is $2.938 \times 10^{67}$ m³, the conversion that carries the survey densities of Section 17.4 into the sphere. In the boundary balance, $\sigma T^4$ has units of W m$^{-2}$ and $NL \div 4\pi R^2$ has units of W m$^{-2}$. They match. In the ice of Section 9, coulombs per meter times one per meter gives coulombs per square meter, a charge per area, and coulombs per square meter times square meters per second gives coulombs per second, which is amperes.

### A.6 Stepping: limits by arithmetic

When a rate changes as time passes, work out the rate right now, apply it for one short step, update, and repeat. Then halve the step and run it again. If the answer barely moves, the steps were small enough. That is the idea of a limit, reached by arithmetic. From Section 9.3: 5-minute steps give 20 minutes, 1-minute steps give 18, 10-second steps give 17.0, and 1-second steps give 16.8. The answer has settled.

### A.7 Reading an equation: three steps, every time

An equation is a compressed sentence. Step one: name every symbol before touching a number. In $\sigma T^4 = NL \div 4\pi R^2$, σ is the Stefan-Boltzmann constant, $5.67 \times 10^{-8}$; T is the temperature in kelvin, which is what we want; N is the number of stars, $2 \times 10^{22}$; L is the luminosity per star, $3.8 \times 10^{26}$ watts; and R is the boundary radius, $4.4 \times 10^{26}$ meters.

Step two: one operation at a time, written down. Rearrange first, to $T^4 = NL \div (4\pi R^2 \sigma)$, because dividing by $4\pi R^2$ and forgetting σ is the easiest mistake to make here. The numerator is $(2 \times 10^{22}) \times (3.8 \times 10^{26}) = 7.6 \times 10^{48}$. The area is $4 \times 3.1416 \times (4.4 \times 10^{26})^2 = 12.566 \times 1.936 \times 10^{53} = 2.433 \times 10^{54}$. Multiplying by σ gives $1.3795 \times 10^{47}$. Dividing, $7.6 \times 10^{48} \div 1.3795 \times 10^{47} = 55.09$, and the fourth root of 55.09 is 2.7244.

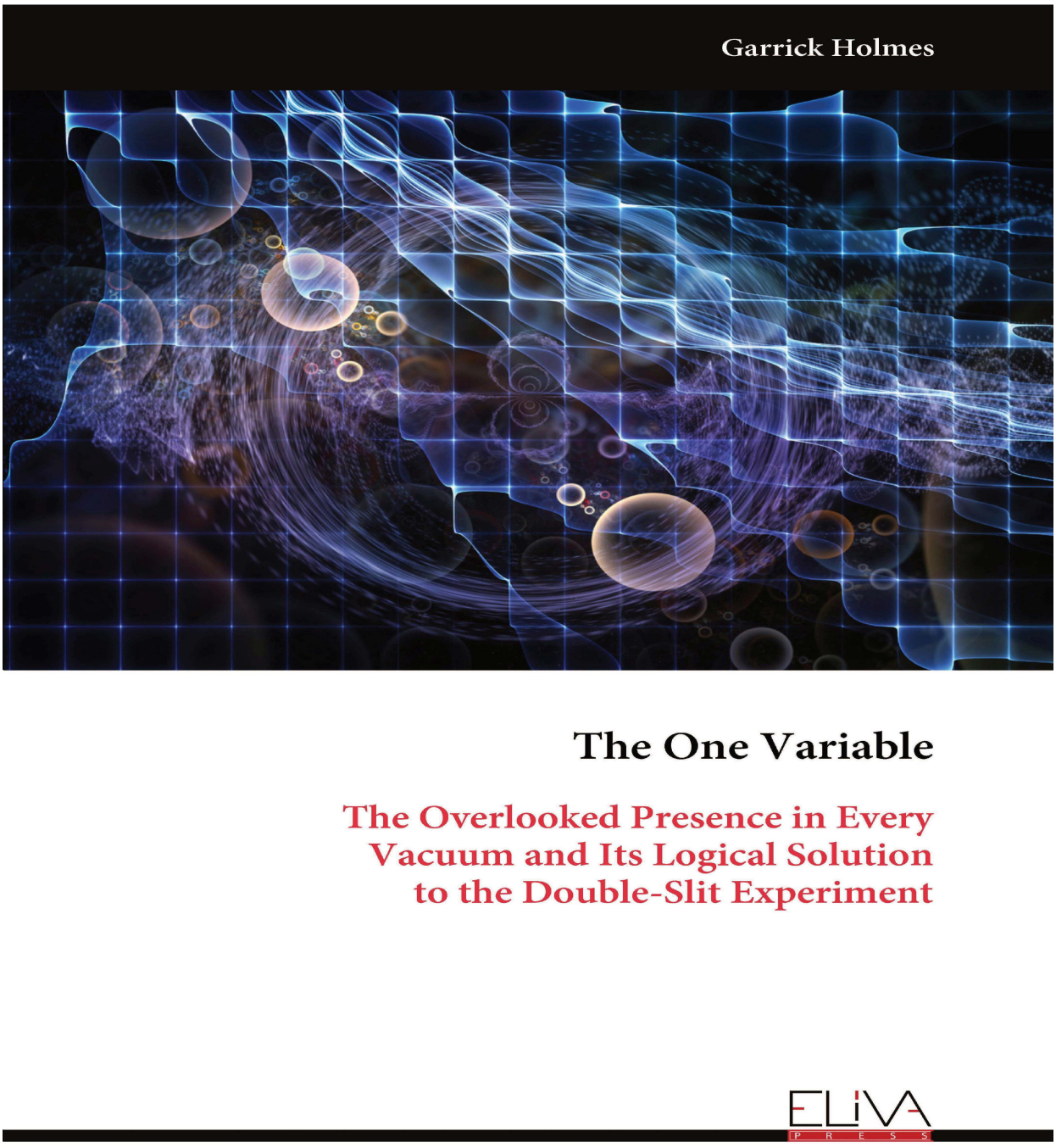
Step three: say the result as a plain sentence. Not “T equals 2.72 K,” which only restates the equation. A real translation: the shell around the observable universe, absorbing the light of twenty thousand billion billion stars, would warm until it glowed at roughly minus 270 degrees Celsius, which is the temperature measured across all of space today. Or, from Section 9.3: a storm's collisions, each leaving less than a femtocoulomb behind, can gather a lightning flash's worth of charge in about seventeen minutes. If you

cannot say it, the calculation is not finished. A sentence that makes no physical sense means something went wrong in step two.

That number, 2.7244 kelvin, came from the tools on these pages. You can check every step. You just did.

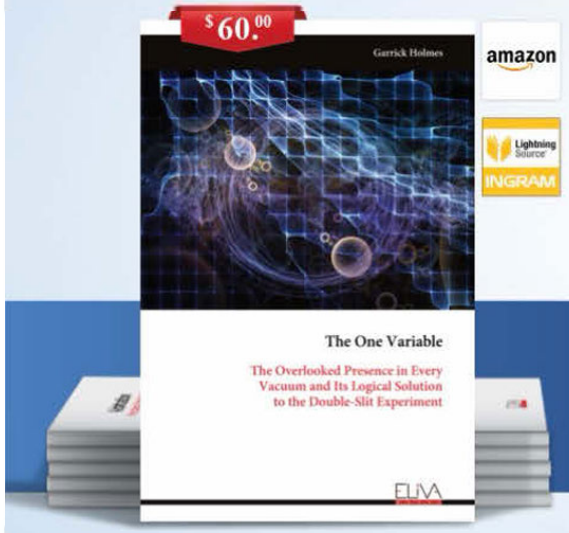
All references can be found in prior articles at the link below

https://www.growkudos.com/profile/garrick_holmes



FOR EVERY 5 COPIES
GET 1 FREE

NEW RELEASE




amazon

Lightning Source
INGRAM

THE ONE VARIABLE

The Overlooked Presence in Every Vacuum and Its Logical Solution to the Double-Slit Experiment

GARRICK HOLMES

ELiVA

Eliva Press

*Certificate of publication for the book titled:*

**The One Variable**
The Overlooked Presence in Every Vacuum and Its Logical Solution to the Double-Slit Experiment

*Authored by:*

**Garrick Holmes**

**ISBN 978-66-850-0271-3**

ELiVA